JGR Atmospheres

RESEARCH ARTICLE
10.1029/2019JD030700

Special Section:
Winter INvestigation of Transport, Emissions and Reactivity (WINTER)

Comparison of Airborne Reactive Nitrogen Measurements During WINTER

Tamara L. Sparks[1,2], Carlena J. Ebben[1], Paul J. Wooldridge[1], Felipe D. Lopez-Hilfiker[3], Ben H. Lee[3], Joel A. Thornton[3], Erin E. McDuffie[4,5,6,7], Dorothy L. Fibiger[4,8], Steven S. Brown[4], Denise D. Montzka[9], Andrew J. Weinheimer[9], Jason C. Schroder[5,6], Pedro Campuzano-Jost[5,6], Jose L. Jimenez[5,6], and Ronald C. Cohen[1]

[1]Department of Chemistry, University of California, Berkeley, CA, USA, [2]Now at California Department of Public Health, Richmond, CA, USA, [3]Department of Atmospheric Sciences, University of Washington, Seattle, WA, USA, [4]Chemical Sciences Division, Earth System Research Laboratory, NOAA, Boulder, CO, USA, [5]Cooperative Institute for Research in Environmental Sciences, University of Colorado Boulder, Boulder, CO, USA, [6]Department of Chemistry, University of Colorado Boulder, Boulder, CO, USA, [7]Now at Department of Physics and Atmospheric Science, Dalhousie University, Halifax, Nova Scotia, Canada, [8]Now at California Air Resources Board, Sacramento, CA, USA, [9]National Center for Atmospheric Research, Boulder, CO, USA

Key Points:
- Nitrogen oxides are accurately and precisely measured by a number of independent methods
- New chemical ionization approaches compare well with more established methods
- Closure of the NOy budget was observed

Correspondence to:
R. C. Cohen,
rccohen@berkeley.edu

Citation:
Sparks, T. L., Ebben, C. J., Wooldridge, P. J., Lopez-Hilfiker, F. D., Lee, B. H., Thornton, J. A., et al. (2019). Comparison of airborne reactive nitrogen measurements during WINTER. *Journal of Geophysical Research: Atmospheres*, *124*, 10,483–10,502. https://doi.org/10.1029/2019JD030700

Received 25 MAR 2019
Accepted 25 AUG 2019
Accepted article online 29 AUG 2019
Published online 11 OCT 2019

Abstract We present a comparison of instruments measuring nitrogen oxide species from an aircraft during the 2015 Wintertime INvestigation of Transport, Emissions, and Reactivity (WINTER) campaign over the northeast United States. Instrument techniques compared here include chemiluminescence (CL), thermal dissociation laser-induced fluorescence (TD-LIF), cavity ring-down spectroscopy (CRDS), high-resolution time of flight, iodide-adduct chemical ionization mass spectrometry (I^-CIMS), and aerosol mass spectrometry. Species investigated include NO_2, NO, total nitrogen oxides (NO_y), N_2O_5, $ClNO_2$, and HNO_3. Particulate-phase nitrate is also included for comparisons of HNO_3 and NO_y. Instruments generally agreed within reported uncertainties, with individual flights sometimes showing much better agreement than the data set taken as a whole, due to flight-to-flight slope changes. NO measured by CRDS and CL showed an average relative slope of 1.16 ± 0.01 across all flights, which is outside of combined uncertainties. The source of the error was not identified. For NO_2 measured by CRDS and TD-LIF the average was 1.02 ± 0.00; for NO_y measured by CRDS and CL the average was 1.01 ± 0.00; and for N_2O_5 measured by CRDS and I^-CIMS the average was 0.89 ± 0.01. NO_y budget closure to within 20% is demonstrated. We observe nonlinearity in NO_2 and NO_y correlations at concentrations above ~30 ppbv that may be related to the NO discrepancy noted above. For $ClNO_2$ there were significant differences between I^-CIMS and TD-LIF, potentially due in part to the temperature used for thermal dissociation. Although the fraction of particulate nitrate measured by the TD-LIF is not well characterized, it improves comparisons to include particulate measurements.

1. Introduction

Nitrogen oxides, including NO_x ($NO_x \equiv NO + NO_2$) and higher oxides (RO_2NO_2, $RONO_2$, HNO_3, N_2O_5, $ClNO_2$, and other molecules) both influence and are affected by atmospheric oxidation rates. NO is directly emitted by anthropogenic and natural sources and is generally quickly converted to NO_2. The concentrations of NO and NO_2 have direct effects on the production of O_3, a pollutant in the troposphere, and on ambient concentrations of OH and peroxy radicals (e.g., RO_2), molecules which in turn affect the lifetime of NO_x (e.g., Kenagy et al., 2018; Romer et al., 2016). The higher oxides of nitrogen can contribute to aerosol through the formation of condensable organics, inorganic nitrate (e.g., Rollins et al., 2013), and inorganic nitrite in some cases (Guo et al., 2016); serve as terminal sinks or reservoirs of NO_x that are transported downwind of initial emission sources; and are diagnostics of our understanding of emissions and chemistry.

As a consequence of their central role in atmospheric chemistry, many independent approaches to observing NO_x, the higher oxides (collectively known as NO_z), total reactive nitrogen ($NO_y = NO_x + NO_z$), and the aerosol-phase oxidized nitrogen have been developed. Examples include chemiluminescent (CL) detection of NO (Ridley & Grahek, 1990); laser-induced fluorescence (LIF) detection of NO_2 (George & O'Brien, 1991; Thornton et al., 2000); cavity ring-down spectroscopy (CRDS) applied to the

direct detection of NO_2 and NO_3 (Brown, 2003; Wagner et al., 2011); luminol detection of NO_2 (Drummond et al., 1991; Wendel et al., 1983); and chemical ionization mass spectrometry (CIMS) applied to detection of HNO_3 (Neuman et al., 2002), N_2O_5, and $ClNO_2$ (e.g., Kercher et al., 2009), as well as organic nitrates and organic peroxy nitrates (Beaver et al., 2012; Lee et al., 2014), ion chromatography for detection of nitrate and nitrite (Dibb et al., 1996; Orsini et al., 2003), particulate organic nitrate by thermal dissociation-laser-induced-fluorescence (TD-LIF; Rollins et al., 2010) and aerosol mass spectrometry (AMS; e.g., Fry et al., 2013; Kiendler-Scharr et al., 2016), and inorganic nitrate by AMS (e.g., Canagaratna et al., 2007).

In addition to the primary detection of species indicated above, many of these techniques have been coupled to strategies for converting all or selected fractions of NO_y to lower oxides (e.g., NO_3, NO_2, or NO) that can be readily measured. Examples include photolytic conversion of NO_2 to NO (Walega et al., 1991), catalytic conversion of NO_y to NO (Walega et al., 1991), and thermal conversion of classes of NO_z to NO_3, NO_2, or NO (Day et al., 2002; Paul et al., 2009; Thieser et al., 2016; Wagner et al., 2011; Wild et al., 2014).

Some reactive nitrogen species present measurement challenges as the molecules of interest can react on, adsorb, or desorb from the walls of sampling lines or partially thermally dissociate as air is sampled and analyzed. Aerosol sampling efficiency through inlets is difficult to quantify and may be quite different for each inlet/species pair. In particular, aerosol transmission is lower for Teflon inlets designed for gas-phase sampling, due to the loss of charged particles (Deming et al., 2019). Thus, sampling of aerosol NO_y species can affect interpretation of observations and comparison of different instruments. The detected aerosol fraction depends on the ambient size distribution and humidity, as well as the specific aircraft and inlet location (even for the same instrument and physical inlet).

A number of previous papers have compared methods for detection of nitrogen oxides. While the studies listed below are not a comprehensive review of reactive nitrogen intercomparisons, they do represent those that have focused on similar sets of instruments (CIMS, LIF, CL, and CRDS) or those that have taken place in the winter season. For NO_2, comparisons relevant to this work include Thornton et al. (2003) in which LIF and CL detection of NO_2 were found to agree within 5% during the ground-based 1999 Southern Oxidant Study, where NO_2 ranged from 0.75 to 60 ppbv, and Fuchs et al. (2010) who found agreement for NO_2 (with NO_2 up to 75 ppbv) within 3% during the SAPHIR NO3COMP chamber comparison, which included CL, LIF, and three cavity-enhanced absorption techniques. A CRDS comparison with CL sampling ambient air (having NO_2 up to 60 ppbv) for 6 days in 2009 found NO_2 and NO agreed within 1% and 3%, respectively (Fuchs et al., 2009). In a recent paper, Javed et al. (2019) compared LIF, CL, CRDS, LP-DOAS (long-path differential optical absorption spectroscopy), and CE (cavity-enhanced)-DOAS NO_2 instruments at a forested site in Germany. They reported agreement within the experimental limitations and instrumental uncertainties over the ambient concentration range of 0.13 to 22 ppbv.

For higher oxides, comparisons could be made between individual species (e.g., PAN or HNO_3), or grouped species. An example is the laboratory comparison of *n*-propyl nitrate (0 to 20 ppbv) measurements by LIF with thermal dissociation (TD-LIF) and CL using a molybdenum oxide catalytic converter, which found agreement within 1% (Day et al., 2002). During a field study at Blodgett forest (where NO_y ranged from 0.5 to 5 ppbv), the same instruments agreed within 7% for NO_y measurements (Day et al., 2002). Also at Blodgett forest, during the BEARPEX (Biosphere Effects on Aerosol and Photochemistry Experiment) 2009 study, two thirds of the TD-LIF summed organic nitrate measurement (0.05 to 1 ppbv) were accounted for by the CF_3O^- CIMS measurements of individually identified biogenic-derived nitrates, with the remainder one third not identified as individual species but consistent by their mass to contain nitrogen (Beaver et al., 2012). Wooldridge et al. (2010) found TD-LIF sum of PANs and summed measurements of individual PAN species agreed to within 10% for a number of ground-based and airborne campaigns where PAN compounds were generally 0.2 to 2 ppbv, with extreme values up to 8 ppbv. CRDS with thermal dissociation (TD) agreed within 1% with a CL instrument for NO_y (up to 6 ppbv) during the 2013 Southern Oxidant and Aerosol Study and within 14% of a sum of NO_y components at the 2013 Uintah Basin Winter Ozone Study (Wild et al., 2014) where NO_y was generally less than 30 ppbv but did reach 60 ppbv extremes. Some of the latter difference is likely due to the lack of organic nitrate measurements to include in the Uintah Basin Winter Ozone Study sum (Lee et al., 2014).

Table 1
Instrument Details

Instrument	Species	Uncertainty	Detection limit
TD-LIF[a]	NO_2	5%	20 pptv
	$RO_2NO_2 + N_2O_5$	10%	30 pptv
	$RONO_2 + ClNO_2$	25%	49 pptv
	$HNO_3 + NO_3$	25%	65 pptv
	NO_y minus NO	10%	48 pptv
CL[b]	NO	30 pptv ± 10%	
	NO_y	100 pptv ± 50%	
CRDS[c]	NO	4%	35–140 pptv
	NO_2	3%	25–114 pptv
	NO_y	12%	50–380 pptv
	N_2O_5	12%	1.3–4.4 pptv
I^-CIMS[d]	N_2O_5	30%	0.4 pptv
	$ClNO_2$	30%	0.6 pptv
	HNO_3	30%	7.0 pptv
AMS[e]	Particle NO_3^-	35%	11 pptv

Note. Values taken from version R3 1-s merged data files reported for Wintertime INvestigation of Transport, Emissions, and Reactivity (available at data.eol.ucar.edu), except for the more recently updated aerosol mass spectrometry version R2 data. Detection limits are for 1σ, 1 s; except for cavity ring-down spectroscopy, which is 2σ, 1 s; and aerosol mass spectrometry, which is 1σ, 1 min.
[a]Day et al. (2002). [b]Walega et al. (1991). [c]Wagner et al. (2011); Wild et al. (2014). [d]Lee, Lopez-Hilfiker, et al., 2014, Lee et al., 2018. [e]Schroder et al. (2018).

Although these comparisons show that many different approaches to nitrogen oxide detection can deliver measurements that are accurate and cross-calibrated to within a few percent, there remain concerns that different approaches may not be fully consistent with each other and that newer approaches (e.g., I^-CIMS and CRDS) have not been extensively compared to better established methods, particularly during airborne campaigns. The Wintertime INvestigation of Transport, Emissions, and Reactivity (WINTER) field experiment over the northeast United States during February and March 2015 provided an opportunity to compare seven different instruments, which measured one or more constituents of NO_y from aboard the National Center for Atmospheric Research (NCAR)-National Science Foundation (NSF) C-130 aircraft. The lower temperatures of the winter season and the extensive nighttime flying provided a wider range of conditions than prior experiments, particularly those leading to the formation N_2O_5 and $ClNO_2$. In this paper we present instrument intercomparisons of NO, NO_2, NO_y, NO_z, N_2O_5, $ClNO_2$, and HNO_3. Two instruments included O_3 measurements; however, the focus here is confined to nitrogen oxide species. In most cases the agreement is better than the stated uncertainties, an indication that the uncertainties are estimated conservatively.

2. Instruments

The WINTER campaign (www.eol.ucar.edu/field_projects/winter) took place in February and March 2015. Based out of the NASA Langley Research Center in Virginia, 13 research flights with NCAR-NSF C-130 aircraft were conducted over the eastern United States with roughly equal attention given to daytime and nighttime. The instruments used in this study are each described briefly below and summarized in Table 1. After the WINTER campaign, a laboratory experiment in July 2015 was conducted to explore the TD-LIF and I^-CIMS measurements of $ClNO_2$. In these experiments, $ClNO_2$ was produced by reaction of gas-phase N_2O_5 over a NaCl salt bed (Kercher et al., 2009).

2.1. Thermal Dissociation Laser-Induced Fluorescence

NO_2 and other oxidized nitrogen classes were measured by a LIF instrument. (The LIF instrument is often referred to as TD-LIF whether or not the TD step described below is involved.) For WINTER, ambient air was sampled at 4.1 L/min through a 28-cm-long, 0.4-cm i.d., PFA Teflon tube warmed to 45 °C to maximize transmission of HNO_3 and $RONO_2$. The tip was 24 cm from the aircraft outer surface at 90° to the flow. A 532-nm Nd:YAG laser with 20-ns pulses at 15 kHz excites NO_2, and fluorescence >700 nm is imaged onto photon counting modules. Time gating is used to discriminate against laser light scattered from inside the cell, as well as from air molecules and aerosol particles (George & O'Brien, 1991; Thornton et al., 2000). An NO_2 standard (4.39 ppmv, 5% uncertainty, Praxair Certified Standard grade) diluted in zero air to deliver mixing ratios within 0–20 ppbv was used to calibrate the instrument by overflowing the inlet at selected times during the flights. A number of NO_2 standard cylinders are kept in the laboratory and intercompared regularly. Each calibration begins with quickly flowing (and diverting to an exhaust line) enough gas through the regulator to purge it of gas that has been in contact with the regulator internal surfaces for more than a few minutes. In addition, calibrations were done frequently enough to keep the mass flow controller and tubing passivated at the cylinder concentration. A correction for fluorescence quenching by water (which quenches five times faster than nitrogen or oxygen) was applied to the data to account for sampling air with ambient humidity but calibrating with dry mixtures. In addition, an empirical correction for nonlinearity arising from multiple photons arriving in the same time gate being counted as one was fitted to laboratory-generated NO_2 concentrations up to 500 ppbv.

The compound classes $\sum$PNs (total peroxynitrates, RO_2NO_2, which are typically dominated by peroxy-acyl nitrates, $RC(O)O_2NO_2$), $\sum$ANs (total alkyl and multifunctional nitrates, $RONO_2$), and $\sum HNO_3$, were measured by TD and LIF detection of the NO_2 product (Day et al., 2002). These utilize separate fused quartz

tubes heated to T_{PNs} = 190 °C, T_{ANs} = 350 °C, and T_{HNO3} = 540 °C. These temperature set points were determined from previous studies on the range of dissociation temperatures in combination with laboratory studies using the specific setup for WINTER (Wooldridge et al., 2010). At T_{PNs}, all peroxy nitrates will be dissociated (Wooldridge et al., 2010). Also at T_{PNs}, N_2O_5 has been shown to be dissociated to NO_2 and NO_3, resulting in one molecule of NO_2 detected per molecule of N_2O_5 (Fuchs et al., 2012; Wood et al., 2003). At T_{ANs}, in addition to ΣPNs, alkyl and multifunctional nitrates including particle-phase organic nitrate, as well as $ClNO_2$, also dissociate (Wooldridge et al., 2010). At T_{HNO3}, all nitrogen oxides, including HNO_3, particle-phase volatile inorganic nitrate (Day et al., 2002; Wooldridge et al., 2010), and NO_3 (Womack et al., 2017), have dissociated. The largest source of NO_3 is N_2O_5 dissociation. Mixing ratios for each class of compounds are determined by subtracting the mixing ratio of the next lowest temperature channel. That is, $NO_2 = NO_2(T_{ambient})$, $\sum PNs = NO_2(T_{PNs}) - NO_2(T_{ambient})$, $\sum ANs = NO_2(T_{ANs}) - NO_2(T_{PNs})$, $\sum HNO_3 = NO_2(T_{HNO3}) - NO_2(T_{ANs})$. The $NO_2(T_{HNO3})$ individual channel is a measurement of NO_y, excluding NO and HONO (as HONO dissociates into NO, which is not detected here), and is labeled as "NO_y minus NO" in the data set. All heated channels also measure nonrefractory particle-phase nitrogen oxides that are transmitted by the inlet, with particle-phase organic nitrate observed in the $\sum$ANs channel and inorganic nitrate in the $\sum HNO_3$ channel. Particle-bound peroxynitrates would appear with $\sum$PNs, but observations have shown no evidence for their presence.

The uncertainty for NO_2 is ~5%, which includes both the uncertainty in the NO_2 standard and uncertainty in the dilution and delivery. In addition, as detailed in Day et al. (2002), uncertainties in the higher oxides include the uncertainty of subtraction of the signal from lower temperature channels, as well as any sampling, heated channel chemical interferences, and inlet transmission losses. The potential humidity dependence of the inlet losses for $\sum$ANs and $\sum HNO_3$ are not separately quantified but included in the stated uncertainties. We estimate these are 10%, 25%, and 25% for $\sum$PNs, $\sum$ANs, and $\sum HNO_3$, respectively, and 10% for the NO_y minus NO measurement. More precise uncertainty estimates take into account the concentrations of the related species (Day et al., 2002). For example, 1 ppbv of HNO_3 is more uncertain if it is observed along with 50 ppbv NO_2 than with of 0.5 ppbv NO_2. An additional uncertainty term arises if the dissociation of a species group does not occur completely within its temperature bounds for a particular heated tube. For example, it has been reported that a small fraction of $\sum HNO_3$ may dissociate below T_{ANs} and thus appear as $\sum$ANs instead of $\sum HNO_3$ (Pusede et al., 2016 reported 2.5%; Womack et al., 2017, reported 2% to 6%; Thieser et al., 2016, reported 10%; Sobanski et al., 2016, reported <0.5%). Data are available for all WINTER research flights for NO_2 and $\sum$PNs, and all except research flights (RFs) 5–6 for $\sum$ANs, and RFs 2–3, 5–7 for $\sum HNO_3$, and RF03 for NO_y minus NO.

2.2. Chemiluminescence

NO and NO_y were measured using a CL instrument (Ridley & Grahek, 1990). The CL reaction of NO with excess O_3 in a reaction vessel designed to operate at 8–10 Torr with 1,000 sccm flow produces photons that are counted using a dry-ice cooled photomultiplier tube. An NO standard (5% uncertainty) diluted in zero air (Walega et al., 1991) is used to calibrate the instrument in flight. NO_y is detected in a separate channel by catalytic conversion to NO. The gold catalyst is operated at 300 °C, and CO is added to the flow. The catalyst was cleansed preflight by heating the gold surface to 500–550 °C for 30–50 min (Bollinger et al., 1983; Fahey et al., 1986; Walega et al., 1991). A warmed (30 °C) Teflon inlet with a flow rate of 1 slpm is rear-facing to reduce particle intake. Uncertainties for NO and NO_y are 30 pptv ± 10% and 100 pptv ± 50%, respectively. NO and NO_y data are available for all flights except RFs 7, 10, and 11.

2.3. CRDS

NO, NO_2, N_2O_5, and NO_y were measured using a cavity ring-down spectrometer (CRDS). CRD spectroscopy exploits the long path within an optical cavity to achieve high sensitivity in direct absorption. Light that coupled to an optical cavity formed from two high reflectivity mirrors (e.g., $R > 99.99\%$) is rapidly extinguished, leading to a single exponential decay of light intensity exiting the cavity (Brown, 2003). Measurement of the characteristic time constant with and without an absorbing trace gas provides a quantitative measure of the absorber concentration. This instrument is referred to here as CRDS, rather than TD-CRDS, unless the TD component is being emphasized. The CRDS deployed during WINTER measured NO, NO_2, and NO_y in four separate channels by direct absorption of NO_2 at 405 nm (Wild et al., 2014). In the

first channel, NO is quantitatively converted to NO_2 by excess O_3 prior to detection (Fuchs et al., 2009). Ambient NO_2 concentrations measured on the second channel are subtracted to derive ambient concentrations of NO. During WINTER, NO and NO_2 were sampled through a 0.198-cm i.d. Teflon line, held at a constant volumetric flow rate of 2.7 lpm. NO_y is measured as NO_2 on a separate channel after TD in a nichrome-wrapped, 650 °C heated quartz tube inlet, described by Wild et al. (2014). After thermal reduction, excess O_3 is added to quantitatively convert NO to NO_2. Nonrefractory particles that enter the heated inlet are vaporized and any oxidized nitrogen molecules present are converted to NO_2 (Wild et al., 2014; Womack et al., 2017). All measurement channels were zeroed every 3–5 min during WINTER by the overflow addition of zero air at the front of each inlet. Both inlets were downward facing at 90° to the airflow. Calibrations of each channel were conducted before and after each research flight and on non-flight days using standard additions of NO_2 generated by conversion of known quantities of O_3 to NO_2 in excess NO, as described by Washenfelder et al. (2011). These calibrations varied by less than 2% over the course of the campaign.

Instrument uncertainty, error, and lower detection limits were compound dependent. CRDS NO and NO_2 data from RFs 1–4 were scaled to the ratio of CRDS/CL NO_y measurements due to an inlet and zeroing error that affected those flights. Uncertainties on these flights were 9% and 8% for NO and NO_2, respectively. For all remaining flights, the uncertainty for NO and NO_2 were 4% and 3%. Limits of detection during WINTER varied by flight and were between 25–115, 35–140, and 50–380 pptv (2σ, 1 Hz) for NO_2, NO, and NO_y, respectively. These limits include the linear sum of the measurement precision and the variation between zeros. These limits are larger than those quoted in Wild et al. (2014) from ground-based data. CRDS measurement uncertainties of these species were determined from the repeatability in the NO_2 calibration procedure (~3%). An additional 1% uncertainty in the NO measurement is associated with uncertainty in sample dilution from the O_3 addition. The NO_y uncertainty of 12% has been previously determined by Wild et al. (2014) based on in-field comparisons to other NO_y instruments and is consistent with estimated uncertainties in the thermal conversion efficiencies of common NO_y components.

Ambient N_2O_5 concentrations were measured on an additional channel of the CRDS instrument. In the inlet, prior to entering the measurement channel, N_2O_5 is thermally dissociated at 130 °C and then measured as NO_3 via direct absorption at 662 nm (Wagner et al., 2011). Measurement zeros were performed every ~3–7 min during WINTER by the addition of excess NO to chemically convert NO_3 to NO_2. The 0.16-cm i.d. Teflon inlet for N_2O_5 was also downward facing at 90° to the airflow. The CRDS measurement of N_2O_5 was calibrated off-line as described in Fuchs et al. (2008) and Wagner et al. (2011) by the addition of constant N_2O_5, in order to determine the inlet transmission efficiency and thermal conversion efficiency of N_2O_5 in the measurement channel. During WINTER, the uncertainty was 12% with a flight-dependent limit of detection of between 1.3 and 4.4 pptv (2σ, 1 Hz). The total uncertainty of N_2O_5 is subject to uncertainties in the temperature dependence of the NO_3 absorption cross section (σ_{NO3}, used to calculate ambient concentrations from measured ring-down times; ~5%) and variation between individual calibrations (~6.5%).

CRDS NO, NO_2, NO_y, and N_2O_5 data are available for all WINTER flights except for N_2O_5 on RF11.

2.4. Iodide-Adduct Chemical Ionization Mass Spectrometry

A high-resolution time-of-flight chemical ionization mass spectrometer with iodide-adduct ionization (HRToF-CIMS, referred to as I⁻CIMS here) measured N_2O_5, $ClNO_2$, and HNO_3 (Lee et al., 2018; Lee, Lopez-Hilfiker, et al., 2014). Intake is at 22 slpm through a 1.6 cm i.d., 40-cm-long polytetrafluoroethylene Teflon inlet after which compounds are ionized with iodide and then detected according to their mass to charge ratios. The inlet tip had a rear facing 45° cut and was unheated to avoid disturbing the gas-particle equilibrium. Water vapor was added to the ion-molecule reaction region to minimize the effect of ambient humidity variations on sensitivity. A correction factor was applied to account for the small residual water dependence (B. H. Lee et al., 2018). The instrument background was determined by periodic displacement of ambient air with ultrahigh purity nitrogen. An in-flight calibration system produced $^{15}N_2O_5$ (or $Cl^{15}NO_2$ with wetted NaCl bed conversion) from O_3 and a gas cylinder with $^{15}NO_2$. The output was sampled off-line by the independently calibrated CRDS and TD-LIF instruments and found to agree to within 1.3%. For further details see Lee et al. (2018). During WINTER, the 1-s 1-σ limits of detection for N_2O_5, $ClNO_2$,

and HNO_3 were 0.4, 0.6, and 7.0 pptv, respectively, with a calibration uncertainty of 30% for each (Lee et al., 2018).

2.5. Particle-Phase Nitrate

Nitrate from submicron particles (PM_1) was measured by a highly customized Aerodyne high-resolution time-of-flight aerosol mass spectrometer (referred to here as AMS; Canagaratna et al., 2007; DeCarlo et al., 2006; Hu et al., 2017; Knote et al., 2011). Details on the AMS configuration in WINTER can be found in Schroder et al. (2018). Briefly, particles were sampled through an NCAR HIMIL inlet (Stith et al., 2009) at 10 slpm into a pressure-controlled region and then focused with an aerodynamic lens. Nonrefractory particle species are vaporized upon impact with a 600 °C porous tungsten vaporizer under high vacuum, and vapors are ionized by electron ionization. Ions (for particulate nitrate: NO^+, NO_2^+, and HNO_3^+) are then detected by time-of-flight mass spectrometry ($\Delta m/m$~2,500 at m/z 46). Instrument response was calibrated after nearly every flight with monodisperse ammonium nitrate particles, with ambient collection efficiency estimated according to Middlebrook et al. (2012). In mixing ratio units, the average uncertainty and detection limit for 1-min data were 35% and 11 pptv, respectively (Schroder et al., 2018).

Additional particulate nitrate measurements were made by a Particle-Into-Liquid Sampler with ion chromatography (PILS-IC) that measures submicron inorganic nitrate (Orsini et al., 2003) and a particle filter with postflight ion chromatography detection that measures inorganic nitrate in aerosol up to 4 μm in diameter (Dibb et al., 1996, 2000). Guo et al. (2016) and Schroder et al. (2018) show agreement within 43% for these three techniques for particulate nitrate, with disagreements largely attributable to differences in size ranges and type (inorganic vs. organic and refractory vs. volatilizable) detected by each instrument. In addition, the PILS reported that some particulate nitrite was present during WINTER, which could also be part of the difference as the AMS does not distinguish between nitrite and nitrate. Only AMS particle-phase nitrate (data set variable "Nitrate_Inorg") is shown in comparisons below, as comparisons were similar for all three of the nitrate measurements and our emphases here is on the gas phase species.

3. Flight Data Comparisons

The time scales for 1-s data were aligned prior to comparison by synchronizing features in the time series. These shifts were typically less than 2 s. Analysis was done with the 1-s data set for NO_2, NO, and NO_y comparisons and a 1-min average for comparisons involving particulate nitrate. Data are from the merged data sets (Revision 3, available at data.eol.ucar.edu) except for the AMS 1-min time scale data set that was updated after assembly of the merge (also available at data.eol.ucar.edu). All best fit lines are bivariate fits assuming unit weights for each variable.

3.1. NO_2

The comparison between CRDS and LIF measurements of NO_2 is shown in Figure 1. RFs 1–4 are plotted with a separate color (red) as the CRDS data for these flights were scaled to the CRDS/CL NO_y ratio, as discussed earlier. RF13 is also removed due to a period of anomalous NO_x data from one of the instruments (with $NO<0$ and $NO_2>NO_y$). At the highest concentrations (>30 ppbv), there is a slight deviation from linearity with the CRDS slightly higher than the LIF. The degree of nonlinearity varied flight by flight and is more pronounced for flights affected by the CRDS zeroing issue (i.e., RFs 1–4).

Correlations of individual flights are generally better than for the overall comparison. The comparison for RF05 is shown in Figure 2 as an example for a flight with overall excellent agreement (i.e., slope = 1.00). From a time series of RF05 in Panels c and d, however, it can be seen that some, but not all, altitude changes can momentarily perturb the agreement. For each of RFs 5–12, the slopes ranged from 0.97 to 1.04. This confirms that flight-to-flight variations in the correlation slope are larger than variations within each flight. On RFs 1–4 the CRDS inlet issue caused higher uncertainty in that measurement and contributed to differences within a flight of as much as 9% between the two measurements. Panels (e) and (f) in Figure 2 show an expanded view of the two instrument's response to a narrow plume. There is no clear difference in time response for the 1-Hz data reported here. Absolute differences may be attributable to the physical separation of the two inlets (LIF sampling forward and from the right side and CRDS sampling from further aft and the

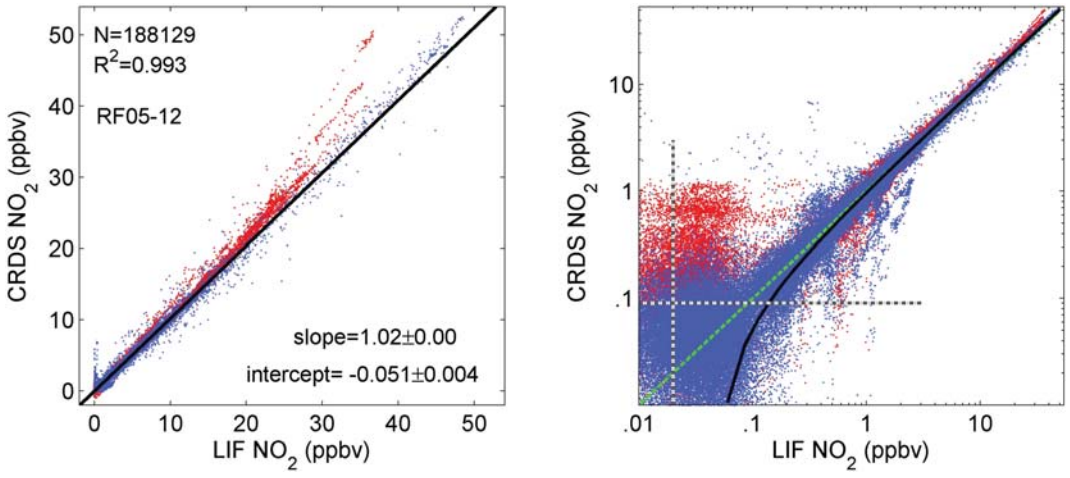

Figure 1. Comparison between cavity ring-down spectroscopy (CRDS) and laser-induced fluorescence (LIF) NO_2 for 1-s data on linear and log scales. Red = RF01 to RF04 and blue = RF05 to RF12. The solid black line is the fit using RF05 to RF12 data, the green dashed line is at 1:1, and the gray dashed lines show the stated detection limits of each instrument (Table 1).

bottom of the aircraft). Overall, the comparison between these two NO_2 instruments suggests that both perform within stated uncertainties but that the LIF NO_2 had better precision during WINTER. The LIF was also calibrated in flight, whereas the CRDS was calibrated between flights.

3.2. NO

The comparison of CRDS and CL for NO, excluding RFs 1–4 and RF13, has slope of 1.16, as shown in Figure 3. Excluding points less than the stated detection limits would yield a slope of 1.15. The fitted intercept was near zero, though the presence of a small offset is apparent in the log-log plot. The slope difference is

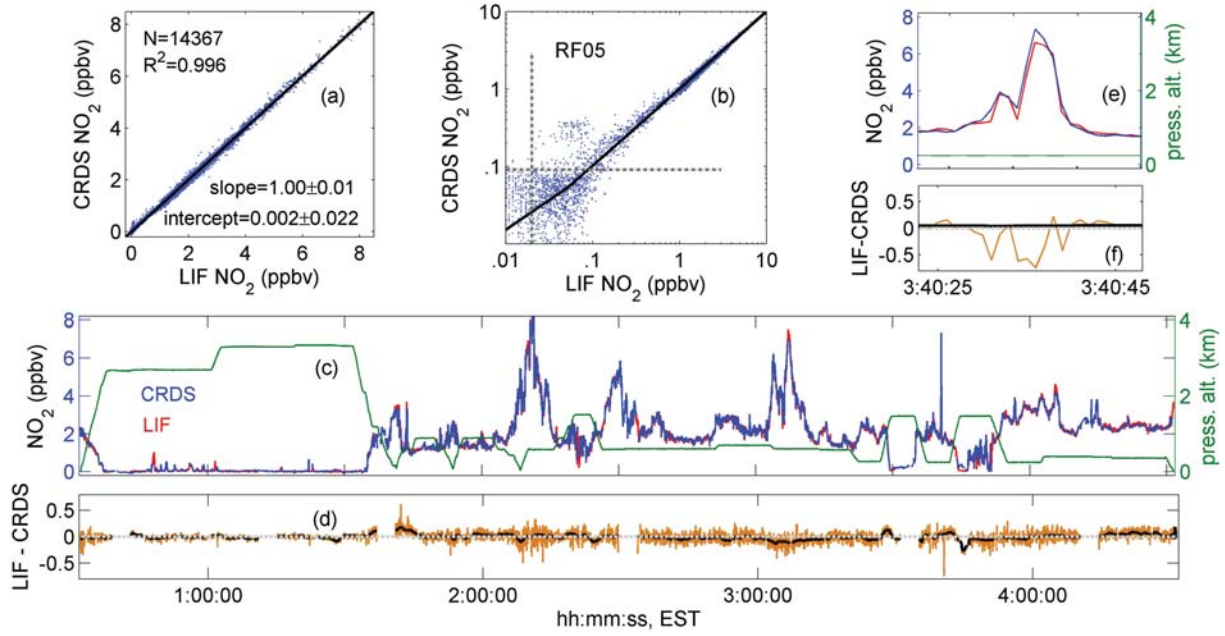

Figure 2. Comparison between cavity ring-down spectroscopy (CRDS) and laser-induced fluorescence (LIF) NO_2 for RF05 on February 23: (a) on a linear scale, (b) on a log scale, (c) as a time series with LIF in red and CRDS in blue, and (d) as ppbv differences of the 1-s (gold) and 1-min (black) averaged data. The black lines in (a) and (b) show the regression slope of 1.00. Gray dashed lines in (b) show the instrument detection limits. The green line in (c) is the aircraft pressure altitude in kilometers above sea level. Panels (e) and (f) show an expanded view of the time series and the difference between the two instruments during the intercept of the narrow plume at 3:40 local time.

larger than the combined instrument uncertainties of 11%. The same two instruments agree better for their measurements of NO_y (discussed below). The NO comparison is linear at the highest concentrations observed. Figure 4 shows a comparison of the measured NO_2/NO ratio from both the CL and CRDS NO instruments to that predicted from a photo-stationary state calculation for a daytime flight (Research Flight 2 over the Ohio River Valley). The measured NO_2/NO ratio uses CRDS NO_2, although the use of LIF NO_2 gives the same result. Calculated $NO_2/NO = k[O_3]/j_{NO2}$, where k is the temperature dependent rate constant for the reaction of NO with O_3 (Sander et al., 2011) and j_{NO2} is the measured photolysis rate constant for NO_2 from a spectroradiometer. Inclusion of the GEOS-Chem model HO_2 from the data merge and assuming $[RO_2] = [HO_2]$ increases the slopes in Figure 4 by at most 1% each. The figure indicates that the CL NO is more consistent with the predicted partitioning of NO_x. Results from other daytime flights are similar. The CL NO measurement, which is not based on a difference, has better precision, and agrees with a photostationary state calculation, is the preferred NO measurement for WINTER.

The NO comparison for RF12 shown in Figure 5 as an example flight that has less scatter than the overall comparison. The slopes for each individual flight excluding RFs 1–4 and RF13 were 1.14 to 1.16 with R^2 values >0.95 with the exception of RF05 (a nighttime-only flight with a single, sharp, NO plume), which had a slope of 1.00 but an R^2 of only 0.16.

3.3. NO_y

There were three NO_y measurements aboard the aircraft during the WINTER campaign: the CRDS NO_y, the CL NO_y measurement, and the TD-LIF measurement of NO_y minus NO. The CRDS versus CL observations for all flight data has a slope of 1.01 ± 0.00 (Figure 6).

The example NO_y comparison from RF06 shown in Figure 7 demonstrates a correlation with little scatter and a slope close to the overall 1:1 correlation. The CL measurement is approximately 2% higher than the CRDS for much of this flight, but this difference is not consistent from flight to flight. The population of points at NO_y near 0.2 ppbv in the CRDS but spanning 0.01–0.1 ppbv in the CL instrument is a period early in the flight (approximately 22:00 to 22:30) when the two instruments show an offset of approximately 0.2 ppbv but are otherwise correlated.

The slopes on each flight vary from 0.93–1.12, all with correlation coefficients of at least 0.98 except for 0.90 for RF13. While the measurements agree within their combined uncertainties for all flights, the interflight variability is larger than for the CRDS versus LIF NO_2 comparison and smaller than the flight-to-flight variance in the CRDS versus CL NO comparison. It is not clear on the basis of this comparison which instrument exhibits greater accuracy, nor the reason for the flight to flight variability. However, the precision on the CL NO_y was generally superior to that of the CRDS (see Table 1).

Since the TD-LIF does not measure NO, the signal from its highest temperature channel, $[NO_2(T_{HNO3})]$, corresponds to NO_y without NO. The TD-LIF "NO_y minus NO" is compared to CRDS and CL measurements in Figure 8. For CL and CRDS, each respective instrument's NO measurement is subtracted from its respective NO_y. The CRDS versus TD-LIF comparison has a slope of 0.94 for the full range of data and 0.91 using just data below 30 ppbv (Figure 8a). Note that restricting the fit range to less than 30 ppbv to avoid the effect of nonlinearity in NO at high concentrations only omits 0.2% of the points. Figure 9 shows one of the periods when the highest NO_y values were sampled (a close transect of a power plant plume) and illustrates the disagreement also appears in NO_z (using CL NO_z = CL NO_y – CL NO – LIF NO_2; using NO_2 from CRDS gives essentially identical results). The lower panel of Figure 9 illustrates that O_x (=O_3 + NO_2) is well conserved in the fresh plume as the O_3 lost to the reaction with NO is regained as NO_2. Section 3.5 below provides a more explicit comparison of the total and speciated NO_z measurements derived from multiple instruments.

3.4. Summary of NO, NO_2, and NO_y Comparisons

Figure 10 provides a summary of the comparisons between the TD-LIF, CRDS, and CL measurements of NO_2, NO, and NO_y on a flight-by-flight basis. Mean comparisons of NO_2 between the LIF and CRDS instruments show agreement within stated uncertainties, both for the average of all comparisons and for the comparisons between individual flights. Both of these instruments appear to adequately represent NO_2 on the scale over which it was observed during WINTER. By contrast, mean comparisons between NO from the CRDS and CL instruments lie outside of the range of combined uncertainties, and this disagreement is

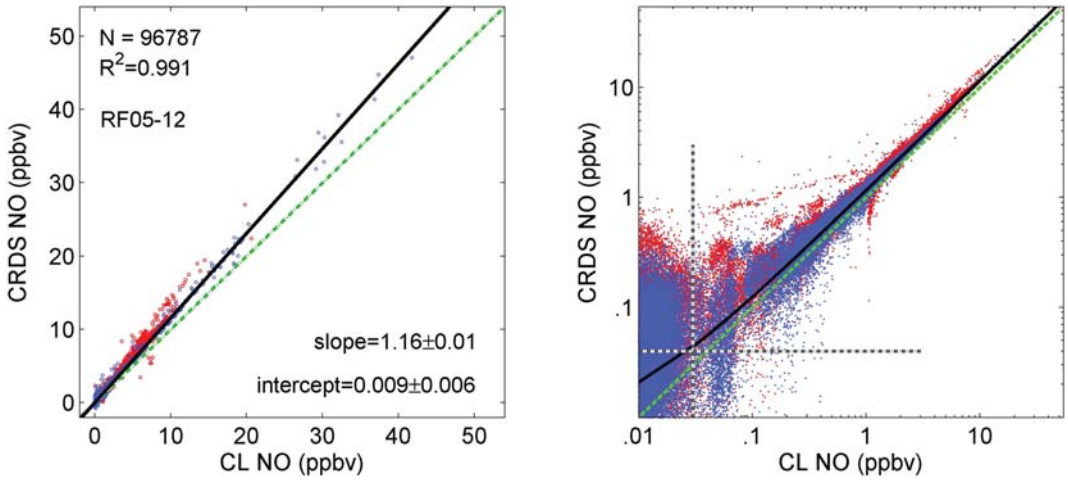

Figure 3. As Figure 1, but for NO. The dashed green line is at 1:1. CL = chemiluminescent.

generally reflected in the flight to flight comparisons. The reason for the discrepancy is unclear, but as described above, it mostly likely lies in the CRDS instrument, since the CL instrument is more consistent with an independent calculation of the NO_2/NO ratio based on a photostationary state argument. Finally, the CRDS to CL comparison for NO_y lies well within the stated, combined uncertainties, both for the mean data and for the flight-to-flight comparisons. The generally better precision for the CL NO_y makes it the preferred data for WINTER. There is no summary figure here that includes the explicit comparison of the TD-LIF NO_y, since that comparison involves subtraction of NO from one of the other instruments (CRDS or CL), as described above. Section 3.6 below discusses the N_2O_5 comparison in Figure 10 in more detail.

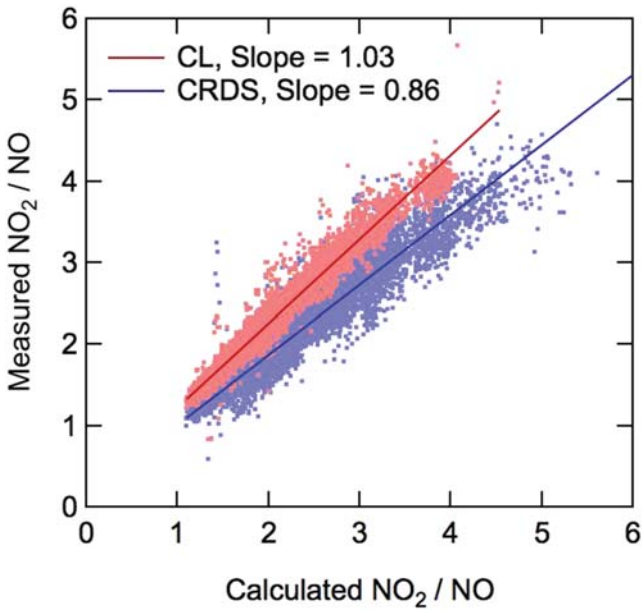

Figure 4. Comparison of measured NO_2/NO for RF02, a daytime flight, to that calculated from a photo-stationary state argument (see text). The measured ratio on the *y* axis uses cavity ring-down spectroscopy (CRDS) NO_2, but the result is the same using laser-induced fluorescence NO_2. The data are filtered for NO > 1 ppbv (both instruments) and solar zenith angle <70° to ensure sunlit conditions. CL = chemiluminescent.

3.5. NO_z (=NO_y−NO_x)

NO_y can be dominated by NO_2 and NO, such that an NO_y comparison is largely a comparison of those species. This can make it difficult to evaluate measurements of more highly oxidized nitrogen compounds. Here, we compare $NO_z = NO_y - NO_2 - NO$ to determine the extent of nitrogen budget closure for higher nitrogen oxides during the WINTER campaign. Nitrogen budgets for two example flights are shown in Figures 11 and 12, which illustrate time series of the principal individually measured components of NO_z during WINTER:

$$\text{speciated } NO_z = 2\times\text{CRDS } N_2O_5 + I^-\text{CIMS } ClNO_2 + I^-\text{CIMS } HNO_3 + \text{AMS } pNO_3$$

along with NO_z measurements from the CRDS, CL, and TD-LIF instruments. (CRDS NO_z = CRDS NO_y − CRDS NO − CRDS NO_2, CL NO_z = CL NO_y − CL NO − CRDS NO_2, and TD-LIF NO_z = $NO_2(T_{HNO3})$ − NO_2 ($T_{ambient}$)). The speciated NO_z sum should be smaller than the NO_y −NO_x measurement, as it does not include peroxy or alkyl nitrates.

An example of a flight with NO_z dominated (70±30%) by HNO_3 is RF06, which took place on February 22–23 off the eastern seaboard throughout the night. Overall, the sum of components tracks well with NO_z (Figure 11); however, the TD-LIF NO_z is noticeably higher than the CRDS and CL NO_z measurements. On average, the sum of NO_z components comprises 105% of CRDS NO_z, 89% of CL NO_z, and 77% of TD-LIF NO_z. At times, N_2O_5 is a substantial portion (averaged 4%, but ranged up to 25%), sometimes but not always coinciding with a rise in $ClNO_2$.

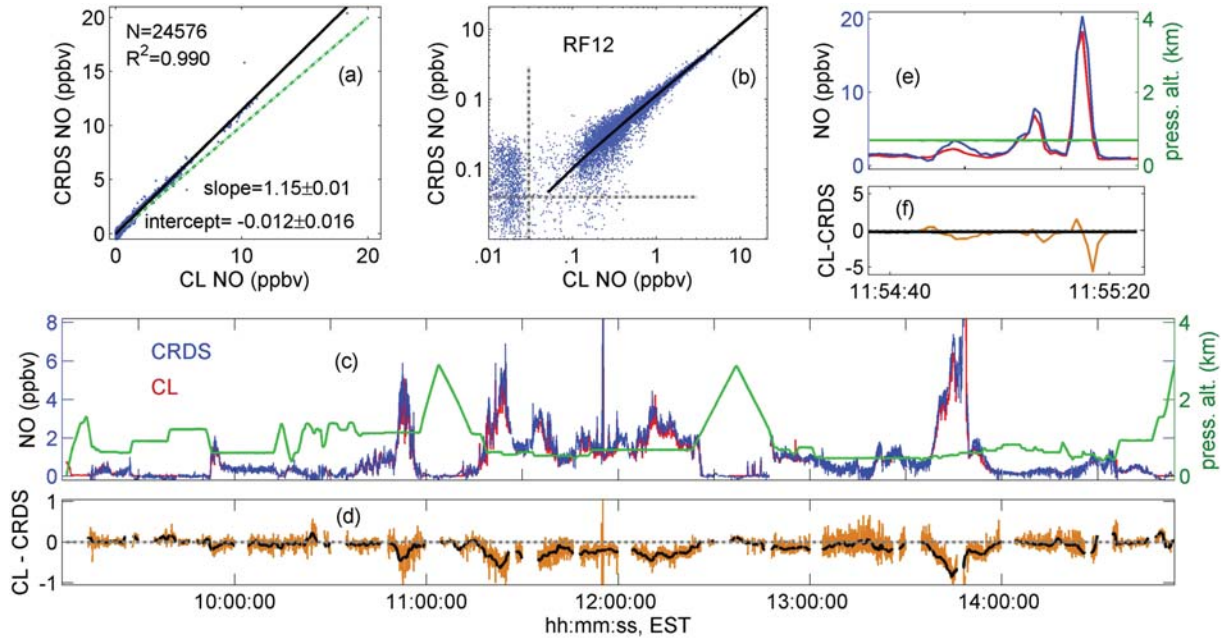

Figure 5. Comparison between cavity ring-down spectroscopy (CRDS) and chemiluminescent (CL) NO for RF12 on 12 March: (a) and (b) are comparison with linear and log scales; (c) has 1-s chemiluminescent (CL) data as red and CRDS as blue; (d) shows the differences of the 1-s (gold) and 1-min (black) averaged data. The (c) *y* axis is clipped from the maximum value of 20.4 ppbv. Panels (e) and (f) show and expanded view of the time series and instrument difference for the narrow plume intercept just prior to 12:00 local time.

Particle-phase nitrate was a small component (5±5%) of NO_z during this flight. This suggests that disagreement is not the result of differences in the aerosol nitrate sampling efficiency of the three NO_y inlets. During this flight, the TD-LIF found that other components (peroxy and alkyl nitrates) contributed little to the total NO_z. Despite variation in total NO_z measurements, NO_z budget closure is demonstrated to within 20% for all flights.

An example flight where the major fractions of NO_z were N_2O_5 and $ClNO_2$ is shown in Figure 12. This was RF08 and took place on 1 March off the eastern seaboard straddling sunrise by a few hours on either side. Agreement between the sum of components with NO_z is slightly better than for RF06, with the sum comprising 98%, 102%, and 81% of NO_z for the CRDS, CL, and TD-LIF instruments, respectively. TD-LIF NO_z is still higher than CRDS and CL, which track more closely to each other than in the prior example. In the early

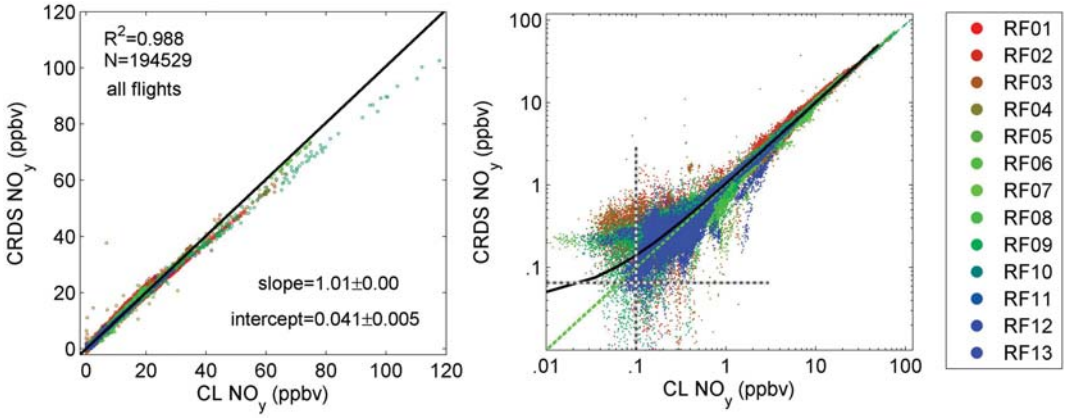

Figure 6. Comparison between cavity ring-down spectroscopy (CRDS) and chemiluminescent (CL) NO_y 1-s data on linear and log scales. The black line is the fitted slope, and the dot-dashed gray lines are the detection limits (Table 1).

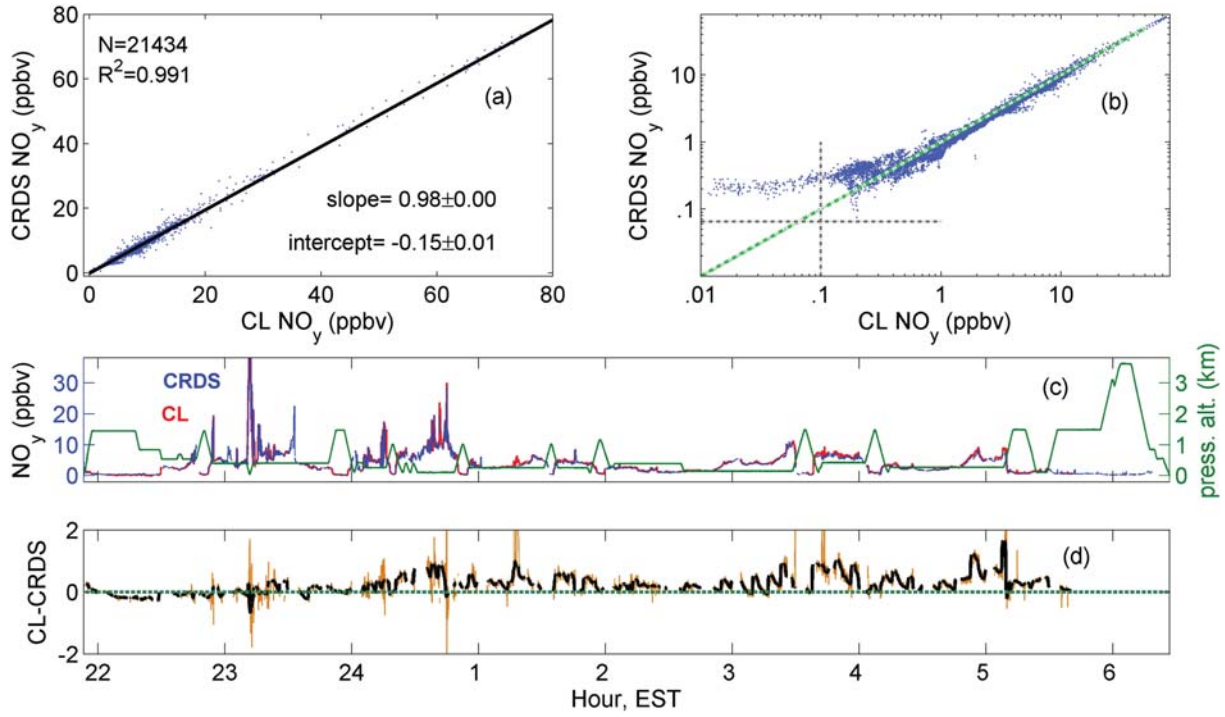

Figure 7. Comparison between cavity ring-down spectroscopy (CRDS) and chemiluminescent (CL) NO_y for RF06 on 23 February: (a) on a linear scale, (b) on a log scale, (c) as a time series, and (d) as ppbv differences of the 1-s (gold) and 1-min (black) averaged data. In (a) the black line shows the fitted slope and in (b) the green line is 1:1 and the gray lines are the detection limits from Table 1. The green line in (c) is the aircraft pressure altitude in km above sea level.

morning before sunrise, N_2O_5 is the dominant component of NO_z (40±5%), but during the hour after sunrise (around 6:30 a.m.), N_2O_5 nearly completely disappears, and HNO_3 becomes dominant. After sunrise, $ClNO_2$ persists longer than N_2O_5. During the 8:00 to 9:00 time period, the N_2O_5 thermal lifetime was approximately 15 min, while the $ClNO_2$ photolysis lifetime was about 2 hr. See McDuffie et al. (2018) for a detailed analysis of $ClNO_2$ during WINTER. Particle-phase nitrate is a larger component of NO_z (30±25%) during this flight, especially after sunrise. Other components of NO_z comprise little of the total for the majority of this flight, with $ClNO_2$ being the next most abundant before sunrise (up to 30%) and HNO_3 gradually becoming dominant after sunrise (up to 70%).

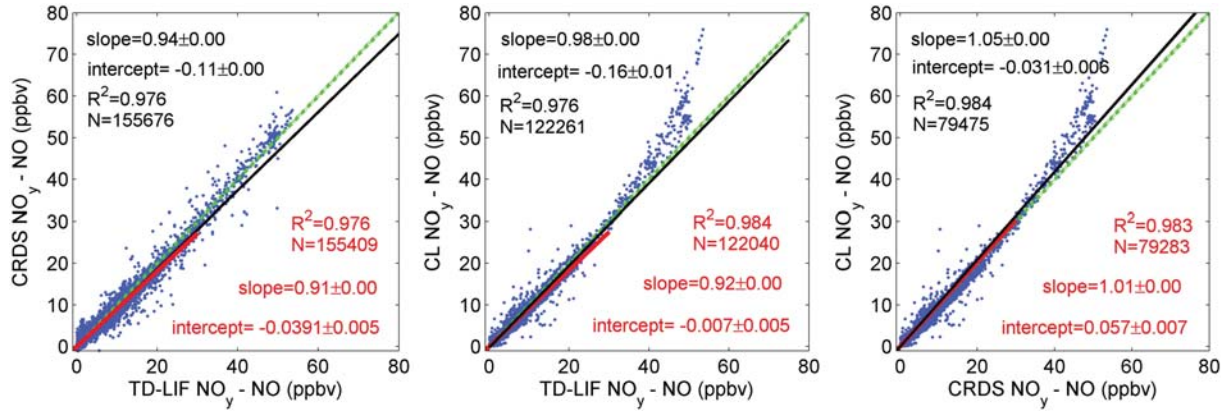

Figure 8. NO_y–NO comparisons between (a) cavity ring-down spectroscopy (CRDS) and thermal-dissociation laser-induced-fluorescence (TD-LIF), (b) chemiluminescent (CL) and TD-LIF, and (c) CL and CRDS. Fits with CRDS exclude RFs 1–4 and 13 as discussed above. The black lines show fits over the full range, and the red lines show fits restricted to <30 ppbv. The green dot-dashed lines are at 1:1.

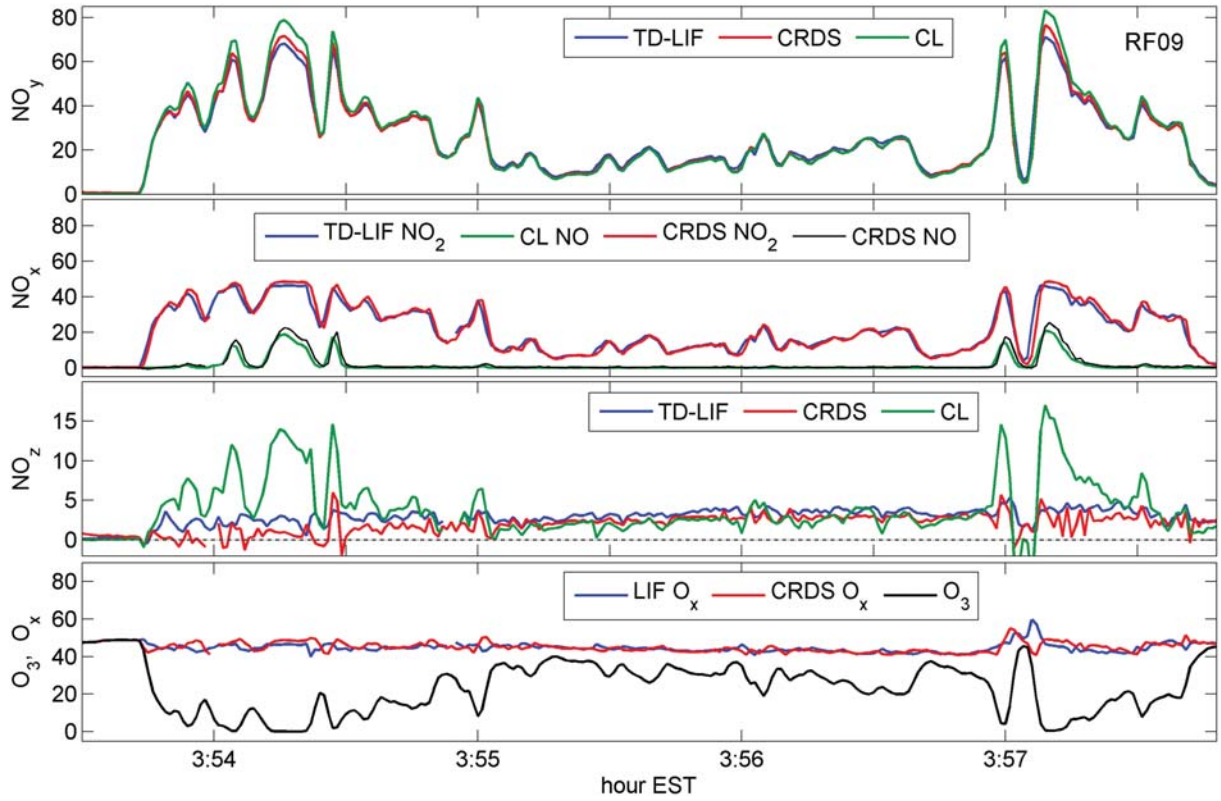

Figure 9. Time series of 1-s data from RF09 illustrating disagreement in NO_y growing above approximately 30 ppbv. All *y* axes are in ppbv. In the top panel thermal-dissociation laser-induced-fluorescence (TD-LIF) NO_y = TD-LIF NO_y minus NO + chemiluminescent (CL) NO. The third panel uses CL NO_z = CL NO_y – CL NO – LIF NO_2. For the bottom panel, O_x are LIF and cavity ring-down spectroscopy (CRDS) NO_2, each plus CL O_3; and the separate O_3 trace is CL O_3.

On the basis of these two comparisons, there is no clear recommendation for NO_z closure. The CRDS and CL total NO_y instruments, with NO_x subtracted, agree with the summed NO_z to within the stated uncertainty of this difference, irrespective of the uncertainty in the sum of speciated components (described in more detail below). The TD-LIF NO_y compared to summed NO_z is outside of the stated uncertainty in Table 1 for the subtraction between the HNO_3 and NO_2 channels. However, the sum is likely to be an underestimate of the total NO_z. Therefore, this comparison shows only that the agreement between total and speciated NO_z is likely within stated uncertainties for all instruments.

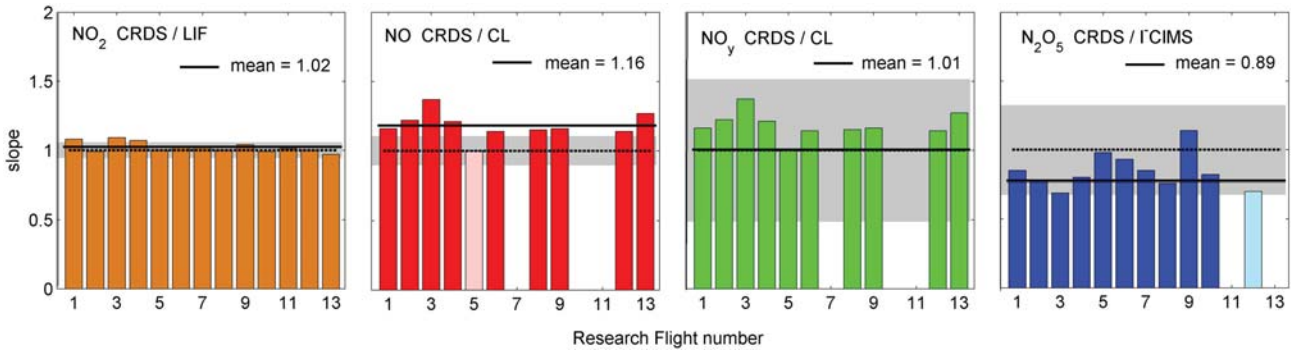

Figure 10. Summary of correlation slopes between instruments measurements of NO_2, NO, NO_y, and N_2O_5 for RFs 1–13. Dotted horizontal lines are at 1:1, gray regions indicate the uncertainties stated in Table 1, and solid black lines are mean relative slopes for the full data set. For RF01–RF12, the NO_2 and NO_y regression coefficients of determination were all >0.98; for NO all were >0.95 except for RF05 (a nighttime-only flight, indicated with a pale red shaded bar); for N_2O_5 all were >0.95 except for RF12 (a daytime-only flight, also with a pale blue shaded bar). CL = chemiluminescent; CRDS = cavity ring-down spectroscopy; LIF = laser-induced-fluorescence; I^-CIMS = iodide-adduct chemical ionization mass spectrometry.

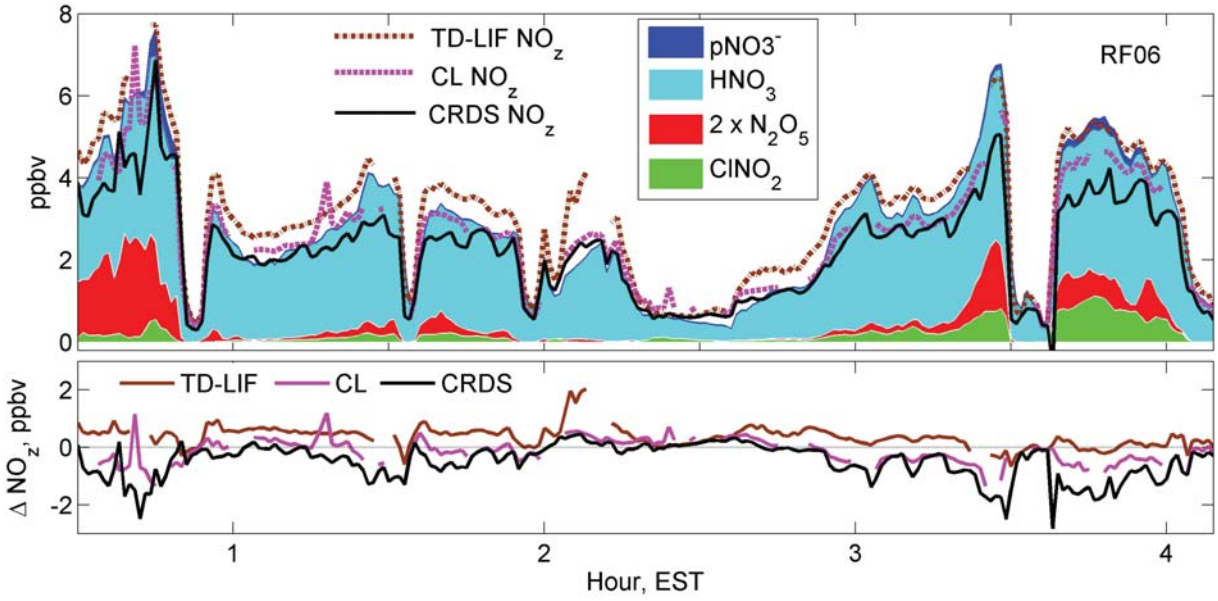

Figure 11. A portion of RF06 on 22–23 February with stacked, speciated NO_z components iodide-adduct chemical ionization mass spectrometry $ClNO_2$, 2 × cavity ring-down spectroscopy (CRDS) N_2O_5, I^-CIMS HNO_3, and AMS particle-phase nitrate (pNO_3^-), along with time series of total NO_z measurements from the CRDS, chemiluminescent (CL), and TD-LIF instruments. The lower panel shows $\Delta NO_z = NO_z - (speciated\ NO_z)$ for the three instruments.

3.6. N_2O_5

Observations of N_2O_5 by CRDS and I^-CIMS from all WINTER flights are compared in Figure 13a and the right panel of Figure 10. A brief comparison of nighttime data only has been presented previously by McDuffie et al. (2018). Across the entire campaign, the slope between CRDS and I^-CIMS was 0.89. Although the R^2 is above 0.95 for most flights, slopes vary from 0.69 to 1.14. A previous, ground-based, comparison of CRDS with I^-CIMS N_2O_5 instruments for a single night in February 2008 showed better agreement over the range of 0–0.9 ppbv, with a slope of 0.98 and an R^2 of 0.97 (Chang et al., 2011).

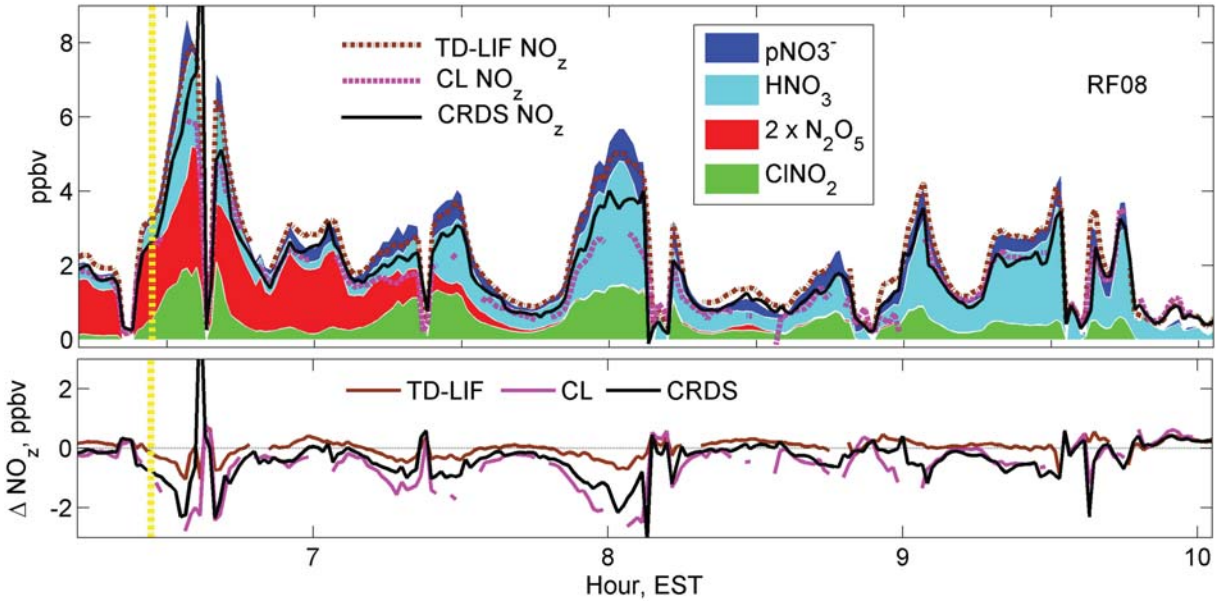

Figure 12. As Figure 11, but for a RF08 on 1 March, which had large NO_z fractions of N_2O_5 and $ClNO_2$. Sunrise is indicated by the vertical yellow line at 6:30. CL = chemiluminescent; CRDS = cavity ring-down spectroscopy; TD-LIF = thermal-dissociation laser-induced-fluorescence; I^-CIMS = iodide-adduct chemical ionization mass spectrometry

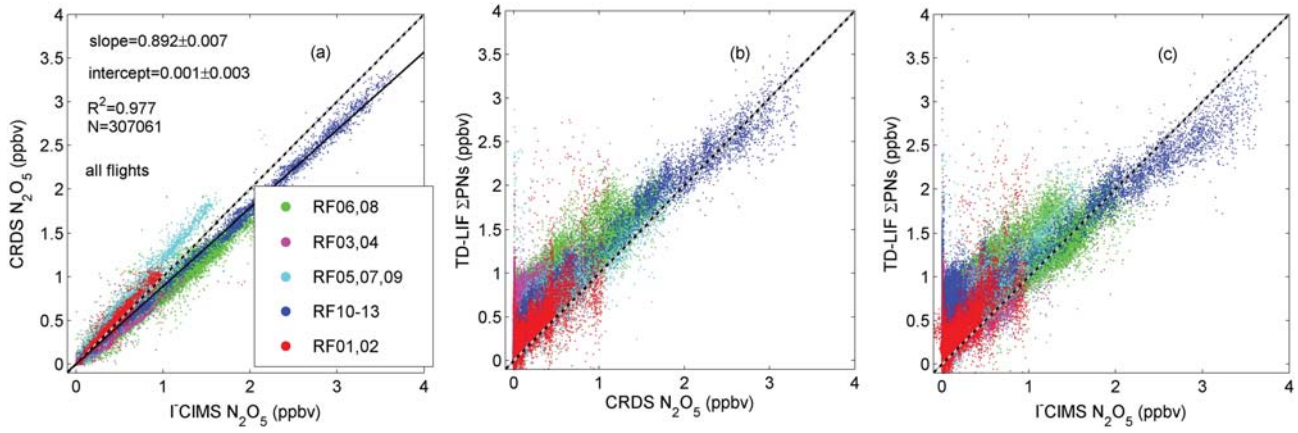

Figure 13. Comparisons for N_2O_5 for all flights between (a) cavity ring-down spectroscopy (CRDS) and iodide-adduct chemical ionization mass spectrometry (I⁻CIMS), and between thermal-dissociation laser-induced-fluorescence (TD-LIF) ∑PNs and (b) CRDS N_2O_5 and (c) I⁻CIMS. Dot-dashed lines indicate 1:1. Color groupings were chosen to highlight single-flight consistency and interflight variations.

N_2O_5 is detected in the TD-LIF ∑PNs difference along with peroxynitrates, and at night during WINTER, a large portion of the signal in this channel is attributable to N_2O_5. Figures 13b and 13c show the comparison of ∑PNs with each N_2O_5 measurement. The points above the lines in Figures 13b and 13c are consistent with presence of peroxynitrates along with N_2O_5, since the TD-LIF measurement includes both. Measurements of ∑PNs − N_2O_5 when N_2O_5 was present (using N_2O_5>0.05 ppbv) were distributed between approximately 0 and 1 ppbv, with a median of 0.22 ppbv, while measurements of ∑PNs when N_2O_5 was not present had a very similar distribution, also with a median of 0.22 ppbv. While the I⁻CIMS reports some higher values than TD-LIF measurements (Figure 13c), scaling the I⁻CIMS measurements by 0.89 to agree with CRDS N_2O_5 would bring the data into agreement with the assumption provided above that ∑PNs will be greater than or equal to N_2O_5.

Although the CRDS and I⁻CIMS instruments agreed generally within stated uncertainties, the disagreement and flight-to-flight variability between the CRDS and I⁻CIMS instruments is worse than in previous, published intercomparisons. The reason for the disagreement is not clear from these data but warrants future investigation and intercomparison activities. The TD-LIF data are more consistent with the CRDS than CIMS, in general, but are themselves subject to potential interference from other species, rendering any conclusion from this comparison exercise uncertain. Use of either the CRDS or CIMS N_2O_5 data from WINTER is recommended, but using the disagreement as a measure of uncertainty, as has been described in the analysis of McDuffie, Fibiger, Dubé, Lopez Hilfiker, et al. (2018).

3.7. $ClNO_2$

$ClNO_2$ is expected to be detected by the TD-LIF in the ∑ANs difference along with $RONO_2$. Using the rate recommended by Baulch et al. (1981), Wooldridge et al. (2010) calculated that $ClNO_2$ would dissociate over a range of 300–425 °C in the TD-LIF ovens, which most closely overlaps with the ∑ANs temperature range of 300–400 °C. Since the dissociation range for HNO_3 was 475–625 °C, with no overlap with the range for $ClNO_2$ or $RONO_2$, there should be a temperature set point at which all $ClNO_2$ will have dissociated while all HNO_3 remains intact. This would completely separate the $ClNO_2$ and HNO_3 signals with $ClNO_2$ detected in the same channel as $RONO_2$. The actual temperature ranges for dissociation depend on the particular oven setup in each experiment, including especially the residence time in the heated section, so experiments are done for each instrument configuration to determine temperature set points in between ranges of dissociation. Thaler et al. (2011) used 450 °C for their TD-cavity ring down $ClNO_2$ instrument, which was the same as the temperature needed for CH_3ONO_2. The shape of the dissociation curve did not match that calculated using the dissociation rate, and the authors speculated that reactions on the heated fused silica surface may have an impact. Thieser et al. (2016), who also used a higher gas flow rate than that used by TD-LIF, observed $ClNO_2$ and $RONO_2$s were fully dissociated by 450 °C. The TD-LIF temperature set

points for WINTER were chosen based on experiments with *n*-propyl nitrate and HNO_3 directly prior to the campaign to determine the best temperature set point to avoid species overlap. Following the campaign, these were verified to still be appropriate.

After the WINTER campaign, additional experiments were conducted in July 2015 with the TD-LIF and I^-CIMS instruments sampling the $ClNO_2$ calibration source (Kercher et al., 2009) in the laboratory. Both instruments sampled air coming from the same oven as the temperature was gradually raised from room temperature to 600 °C. The instrument responses to the heater temperature are opposite, since I^-CIMS measures $ClNO_2$ directly and the TD-LIF measures the NO_2 TD product. Figure 14 plots normalized values and shows 1− I^-CIMS to highlight the comparison. The TD-LIF response to $RONO_2$ (*n*-propyl nitrate) from a separate experiment is also shown. The $ClNO_2$ responses versus temperature do not track together completely; instead, TD-LIF signal flattens before the I^-CIMS signal does. The dotted line at 350 °C indicates the temperature set point used during WINTER.

For the TD-LIF, $ClNO_2$ appears to dissociate fully by 350 °C, suggesting that all $ClNO_2$ would be observed in ∑ANs. However, the temperature for full dissociation observed by the I^-CIMS is 400 °C. The difference should not be due to gas-phase recombination of NO_2 and Cl because Cl atoms react very rapidly even with background levels of methane, etc. For example, the calculated Cl atom lifetime in the presence of 1.9 ppmv CH4 is <25 ms at 350 °C, which is short compared to the 50-ms residence time in the heated section. An alternate explanation for the difference could be surface reactions in the tubing, as the tubing from the oven to each instrument was of different lengths. This suggests that all the $ClNO_2$ would be observed in ∑ANs, but the temperature set point is marginally too low and some portion of $ClNO_2$ may be observed as $\sum HNO_3$.

Observations during WINTER, however, show periods of time where the I^-CIMS $ClNO_2$ measurement is higher than ∑ANs, which should include total $RONO_2$ + $ClNO_2$. Figure 15 shows a time series where this is the case from RF08, during which some of the highest $ClNO_2$ concentrations were observed.

Given that the temperature set point was on the edge of $ClNO_2$ dissociation, a possible explanation is that some $ClNO_2$ was not dissociated at that temperature and was detected instead in the hotter $\sum HNO_3$ channel. To explore this possibility, in Figure 15 we compare the sum of ∑ANs and $\sum HNO_3$ with the sum of their major components, $ClNO_2$, HNO_3, and N_2O_5, to determine if the gap persists or is closed. However, the ∑ANs – $ClNO_2$ difference (Panel b) largely persists with the (∑ANs+$\sum HNO_3$) − ($ClNO_2$+HNO_3+N_2O_5) difference (Panel d), suggesting the temperature set point was not the principal reason for the disagreement on this day.

The proportion of $ClNO_2$ signal that is not seen in the ∑ANs measurement was variable during WINTER. For measurements where $ClNO_2$ is at least 100 pptv, the median ∑ANs signal as a percentage of total $ClNO_2$ is 67% but varied widely with a standard deviation of 55%. Due to this $ClNO_2$ measurement discrepancy, data were not reported for ∑ANs or $\sum HNO_3$ during WINTER when $ClNO_2$ was present above 0.05 ppbv. We further note that the ∑ANs may be subject to an interference from the fraction of HNO_3 that dissociates at the set temperature of the ∑ANs channel oven (Womack et al., 2017). As there were no other ∑ANs measurement against which to compare, this paper does not attempt to assess the accuracy relative to other instruments of the ∑ANs measurement from WINTER.

3.8. HNO_3

The TD-LIF $\sum HNO_3$ measurement includes gas-phase HNO_3, any nonrefractory inorganic particulate-phase nitrate that is sampled through the inlet tubing, and NO_3 dissociation (where the NO_3 is primarily from $N_2O_5 \rightarrow NO_2+NO_3$; Womack et al., 2017). To compare $\sum HNO_3$ to I^-CIMS HNO_3, we select data when N_2O_5 is less than 50 pptv. Figure 16a shows the comparison of TD-LIF $\sum HNO_3$ with I^-CIMS HNO_3 with an overall slope of 0.76 where the TD-LIF is higher than CIMS. The same comparison but to I^-CIMS HNO_3 + pNO_3^- shown in Figure 16b has a slope of 1.02 and a higher R^2. The improvement in correlation when including the particulate nitrate suggests that the TD-LIF observes most of the submicron nitrate aerosol. The efficiency of sampling of nitrate aerosol by NO_y inlets is an important analytical issue for these instruments. We expect a high sampling efficiency for submicron aerosol for the TD-LIF inlet described in section 2.1 but that has not been verified experimentally. For the wintertime DISCOVER-AQ study in the

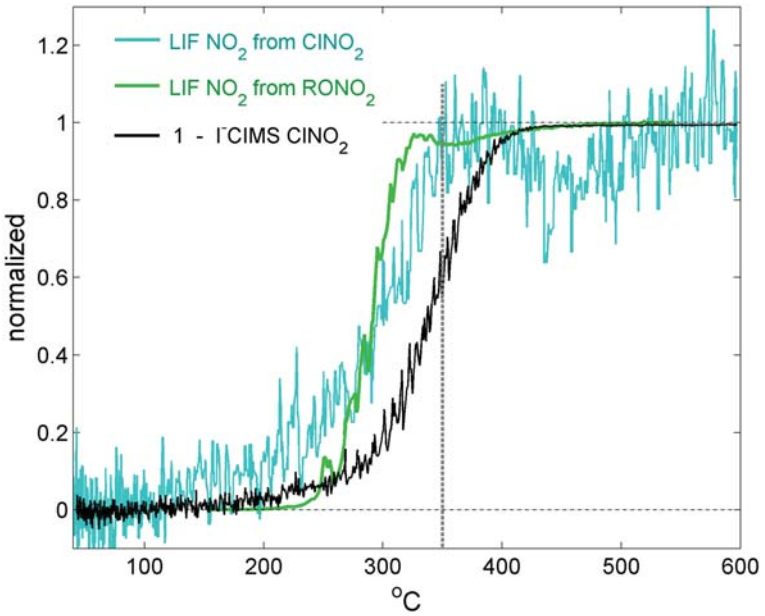

Figure 14. Thermal-dissociation laser-induced-fluorescence (TD-LIF) and iodide-adduct chemical ionization mass spectrometry (I^-CIMS) response to a $ClNO_2$ source versus temperature; overlaid with the TD-LIF response to $RONO_2$ (*n*-propyl nitrate). The unnormalized TD-LIF signal range was 0.30 to 0.72 ppbv. The vertical line indicates the 350 °C oven tube set point temperature used during Wintertime INvestigation of Transport, Emissions, and Reactivity.

California San Joaquin Valley, Pusede et al. (2016) fitted a slope of 0.8 to the TD-LIF $\sum HNO_3$ versus PILS-IC NO_3^- relationship, which was within the combined 25% uncertainty of the two measurements. The measured NH_3 was in excess of $\sum HNO_3$ during that study. Data from WINTER also suggest efficient sampling of particulate nitrate, at least for the configuration of the TD-LIF inlet, but are not conclusive. Further intercomparison of instruments measuring both NO_y and nitrate aerosol is recommended in regions where particulate nitrate comprises a large fraction of NO_z.

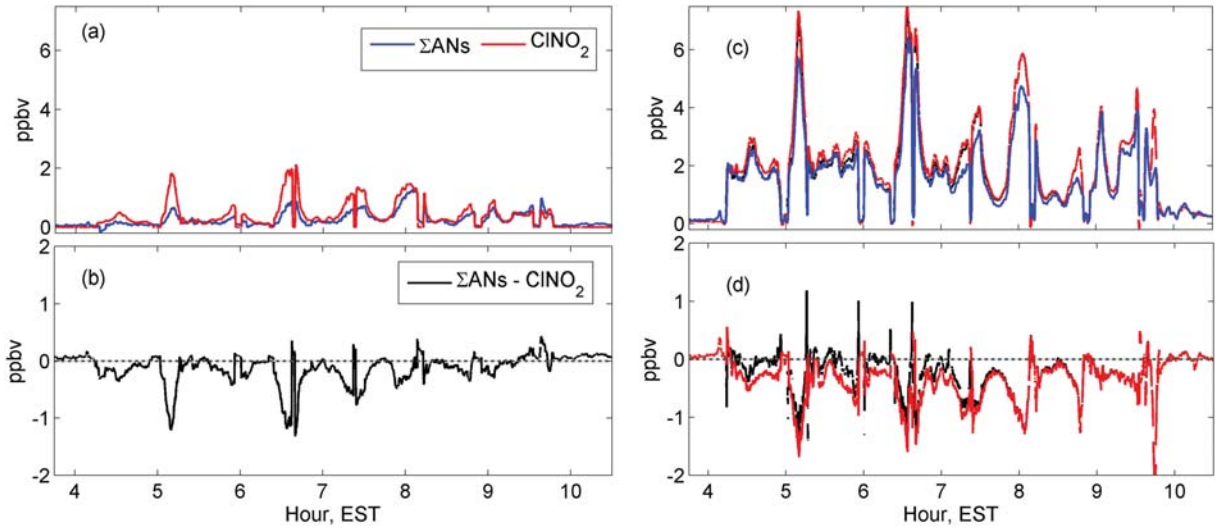

Figure 15. Time series for RF08 with (a) thermal-dissociation laser-induced-fluorescence (TD-LIF) $\sum$ANs (blue) and iodide-adduct chemical ionization mass spectrometry (I^-CIMS) $ClNO_2$ (red), (b) the $\sum$ANs − $ClNO_2$ difference (black), (c) TD-LIF $\sum$ANs+$\sum HNO_3$ (blue) and comparable sums $ClNO_2$+HNO_3+N_2O_5+pNO_3^- using CRDS N_2O_5 (black) and I^-CIMS N_2O_5 (red), and (d) the ($\sum$ANs+$\sum HNO_3$) – ($ClNO_2$+HNO_3+N_2O_5+pNO_3^-) difference with red and black as in (c).

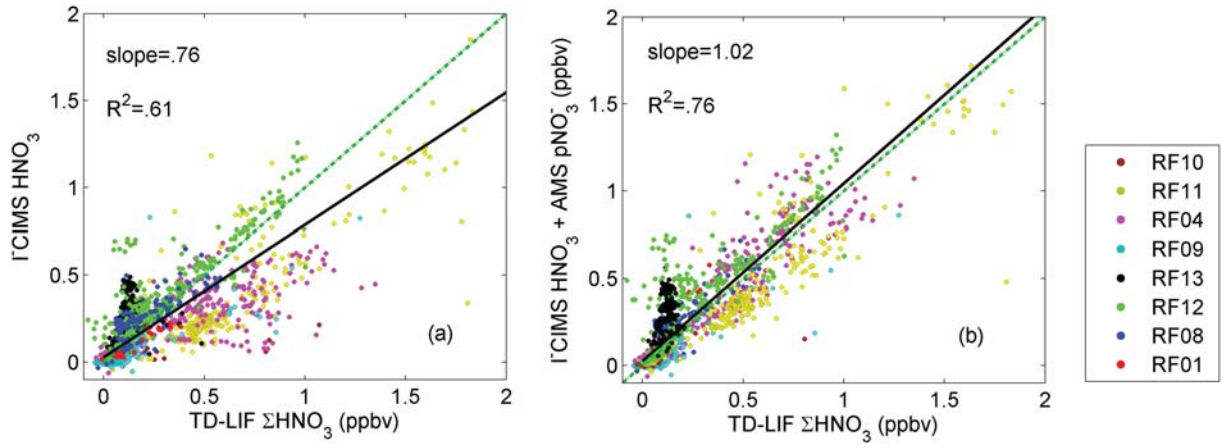

Figure 16. Comparison of thermal-dissociation laser-induced-fluorescence (TD-LIF) $\sum HNO_3$ with iodide-adduct chemical ionization mass spectrometry (I^-CIMS) HNO_3 for flights with mutually reported data. The green dashed line indicates a 1:1 correlation and the solid line is the fit. Data were selected for $N_2O_5 < 50$ pptv.

4. Conclusions

The comparisons here indicate that instruments used during WINTER for measurements of nitrogen oxides are consistent with each other to within 20% or better. Often, correlations agree better than the combined instrument uncertainty, indicating that the reported uncertainties of individual instruments are conservative estimates. For most species, agreement within an individual flight was better than for the comparison of all campaign data. Measurements at mixing ratios that are close to instrument detection limits were not a focus of this campaign. Based on the analysis above, we make the following summary statements/recommendations. These recommendations are specific to the WINTER campaign and are not intended as general recommendations for other intercomparisons.

1. Comparison of CRDS and LIF NO_2 showed agreement to within stated uncertainties both in the average and the flight to flight comparisons. Both measurements are considered reliable for WINTER.
2. Comparison of CRDS and CL NO was outside of stated uncertainties. A cross check against a photostationary state calculation suggests the error is in the CRDS NO measurement, although we are unable to identify the cause of such an error. Thus, the CL NO measurement, where it is available, is recommended for WINTER.
3. Comparison of CRDS and CL NO_y measurements agree within stated uncertainties, such that either measurement may be considered reliable for WINTER. The precision of the CL NO_y measurement was in general superior. The TD-LIF instrument measured the sum of all NO_y components except for NO. Comparison to the CRDS NO_y−NO and CL NO_y−NO showed agreement to well within stated uncertainties below 30 ppbv, but a nonlinear relationship above this level that may be related to the uncertainty in the CRDS NO noted above.
4. Closure of the NO_z (NO_y−NO_x) budget between the total NO_y instruments and the sum of the major speciated components agreed to within 20%. There is no recommendation for a preferred/more accurate instrument.
5. Comparison of CRDS and I^-CIMS N_2O_5 showed agreement to within stated uncertainties but considerable variability from flight to flight that is not explained here. The comparison was not as good as previous, published intercomparisons. While the TD-CRDS has an inherent, stable instrument response in that it is a direct absorption measurement, the I^-CIMS was routinely calibrated and did not show variation that could explain the discrepancy. Therefore, we recommend further field or lab inter-comparison of these instruments.
6. In prior TD-LIF deployments, conditions favoring the formation of N_2O_5 and $ClNO_2$ were very rare, but such conditions were specifically targeted during WINTER. We found evidence that the $ClNO_2$ signal was not entirely observed in the expected channel on the TD-LIF instrument. Further characterization of the TD behavior of $ClNO_2$ is needed.

7. While the efficiency of in-flight particulate nitrate sampling by the TD-LIF was not quantified, including particulate nitrate brings the overall TD-LIF $\sum HNO_3$ versus I^-CIMS HNO_3 comparison into agreement to within 2%.

Acknowledgments
We thank the NSF/NCAR Research Aircraft Facility engineers, scientists, pilots, staff members, and the entire WINTER science team. T. L. S., C. J. E., P. J. W, and R. C. C. acknowledge funding from NSF AGS-1360761; J. A. T., F. L-H., and B. H. L. acknowledge funding from NSF AGS-1360745; J. C. S., P. C-J., and J. L. J. acknowledge funding from NSF AGS-1822664 and NASA NNX15AT96G; S. S. B. and E. E. M. acknowledge support from the NOAA Atmospheric Chemistry, Climate and Carbon Cycle (AC4) Program. Funding for D. L. F. was provided by NSF Award 1433358. The National Center for Atmospheric Research is sponsored by the National Science Foundation. Any opinions, findings, and conclusions or recommendations expressed in this publication are those of the authors and do not necessarily reflect the views of the National Science Foundation. WINTER data are available on the NCAR website (https://data.eol.ucar.edu/master_list/?project=WINTER).

References

Baulch, D. L., Duxbury, J., Grant, S. J., & Montague, D. C. (1981). Evaluated kinetic data for high temperature reactions, Volume 4, Homogeneous gas phase reactions of halogen- and cyanide-containing species. *Journal of Physical and Chemical Reference Data*, *10*(1), 1–721.

Beaver, M. R., Clair, J. M. S., Paulot, F., Spencer, K. M., Crounse, J. D., LaFranchi, B. W., et al. (2012). Importance of biogenic precursors to the budget of organic nitrates: Observations of multifunctional organic nitrates by CIMS and TD-LIF during BEARPEX 2009. *Atmospheric Chemistry and Physics*, *12*(13), 5773–5785. https://doi.org/10.5194/acp-12-5773-2012

Bollinger, M. J., Sievers, R. E., Fahey, D. W., & Fehsenfeld, F. C. (1983). Conversion of nitrogen dioxide, nitric acid, and n-propyl nitrate to nitric oxide by gold-catalyzed reduction with carbon monoxide. *Analytical Chemistry*, *55*(12), 1980–1986. https://doi.org/10.1021/ac00262a034

Brown, S. S. (2003). Absorption spectroscopy in high-finesse cavities for atmospheric studies. *Chemical Reviews*, *103*(12), 5219–5238. https://doi.org/10.1021/cr020645c

Canagaratna, M. R., Jayne, J. T., Jimenez, J. L., Allan, J. D., Alfarra, M. R., Zhang, Q., et al. (2007). Chemical and microphysical characterization of ambient aerosols with the aerodyne aerosol mass spectrometer. *Mass Spectrometry Reviews*, *26*(2), 185–222. https://doi.org/10.1002/mas.20115

Chang, W. L., Bhave, P. V., Brown, S. S., Riemer, N., Stutz, J., & Dabdub, D. (2011). Heterogeneous atmospheric chemistry, ambient measurements, and model calculations of N_2O_5: A review. *Aerosol Science and Technology*, *45*(6), 665–695. https://doi.org/10.1080/02786826.2010.551672

Day, D. A., Wooldridge, P. J., Dillon, M. B., Thornton, J. A., & Cohen, R. C. (2002). A thermal dissociation laser-induced fluorescence instrument for in situ detection of NO_2, peroxy nitrates, alkyl nitrates, and HNO_3. *Journal of Geophysical Research*, *107*(D6), 4046. https://doi.org/10.1029/2001JD000779

DeCarlo, P. F., Kimmel, J. R., Trimborn, A., Northway, M. J., Jayne, J. T., Aiken, A. C., et al. (2006). Field-deployable, high-resolution, time-of-flight aerosol mass spectrometer. *Analytical Chemistry*, *78*(24), 8281–8289. https://doi.org/10.1021/ac061249n

Deming, B., Pagonis, D., Liu, X., Day, D., Talukdar, R., Krechmer, J., et al. (2019). Measurements of delays of gas-phase compounds in a wide variety of tubing materials due to gas-wall interactions. *Atmospheric Measurement Techniques*, 1–19. https://doi.org/10.5194/amt-2019-25

Dibb, J. E., Talbot, R. W., Klemm, K. I., Gregory, G. L., Singh, H. B., Bradshaw, J. D., & Sandholm, S. T. (1996). Asian influence over the western North Pacific during the fall season: Inferences from lead 210, soluble ionic species and ozone. *Journal of Geophysical Research*, *101*(D1), 1779–1792. https://doi.org/10.1029/94JD03117

Dibb, J. E., Talbot, R. W., & Scheuer, E. M. (2000). Composition and distribution of aerosols over the North Atlantic during the Subsonic Assessment Ozone and Nitrogen Oxide Experiment (SONEX). *Journal of Geophysical Research*, *105*(D3), 3709–3717. https://doi.org/10.1029/1999JD900424

Drummond, J., Mackay, G. I., & Schiff, H. I. (1991). Measurement of peroxyacetyl nitrate, N02, and NOx by using a gas chromatograph with a luminol-based detector. Proc. SPIE 1433, Measurement of Atmospheric Gases, 242–252. https://doi.org/10.1117/12.46168

Fahey, D. W., Hübler, G., Parrish, D. D., Williams, E. J., Norton, R. B., Ridley, B. A., et al. (1986). Reactive nitrogen species in the troposphere: Measurements of NO, NO_2, HNO_3, particulate nitrate, peroxyacetyl nitrate (PAN), O_3, and total reactive odd nitrogen (NO_y) at Niwot Ridge, Colorado. *Journal of Geophysical Research*, *91*(D9), 9781–9793. https://doi.org/10.1029/JD091iD09p09781

Fry, J. L., Draper, D. C., Zarzana, K. J., Campuzano-Jost, P., Day, D. A., Jimenez, J. L., et al. (2013). Observations of gas- and aerosol-phase organic nitrates at BEACHON-RoMBAS 2011. *Atmospheric Chemistry and Physics*, *13*(17), 8585–8605. https://doi.org/10.5194/acp-13-8585-2013

Fuchs, H., Ball, S. M., Bohn, B., Brauers, T., Cohen, R. C., Dorn, H.-P., et al. (2010). Intercomparison of measurements of NO_2 concentrations in the atmosphere simulation chamber SAPHIR during the NO3Comp campaign. *Atmospheric Measurement Techniques*, *3*(1), 21–37. https://doi.org/10.5194/amt-3-21-2010

Fuchs, H., Dubé, W. P., Ciciora, S. J., & Brown, S. S. (2008). Determination of inlet transmission and conversion efficiencies for in situ measurements of the nocturnal nitrogen oxides, NO_3, N_2O_5, and NO_2, via pulsed cavity ring-down spectroscopy. *Analytical Chemistry*, *80*(15), 6010–6017. https://doi.org/10.1021/ac8007253

Fuchs, H., Dubé, W. P., Lerner, B. M., Wagner, N. L., Williams, E. J., & Brown, S. S. (2009). A sensitive and versatile detector for atmospheric NO_2 and NO_x based on blue diode laser cavity ring-down spectroscopy. *Environmental Science & Technology*, *43*(20), 7831–7836. https://doi.org/10.1021/es902067h

Fuchs, H., Simpson, W. R., Apodaca, R. L., Brauers, T., Cohen, R. C., Crowley, J. N., et al. (2012). Comparison of N_2O_5 mixing ratios during NO3Comp 2007 in SAPHIR. *Atmospheric Measurement Techniques*, *5*(11), 2763–2777. https://doi.org/10.5194/amt-5-2763-2012

George, L. A., & O'Brien, R. J. (1991). Prototype FAGE determination of NO_2. *Journal of Atmospheric Chemistry*, *12*(3), 195–209. https://doi.org/10.1007/BF00048073

Guo, H., Sullivan, A. P., Campuzano-Jost, P., Schroder, J. C., Lopez-Hilfiker, F. D., Dibb, J. E., et al. (2016). Fine particle pH and the partitioning of nitric acid during winter in the northeastern United States. *Journal of Geophysical Research: Atmospheres*, *121*, 10,355–10,376. https://doi.org/10.1002/2016JD025311

Hu, W., Campuzano-Jost, P., Day, D. A., Croteau, P., Canagaratna, M. R., Jayne, J. T., et al. (2017). Evaluation of the new capture vapourizer for aerosol mass spectrometers (AMS) through laboratory studies of inorganic species. *Atmospheric Measurement Techniques*, *10*(8), 2897–2921. https://doi.org/10.5194/amt-10-2897-2017

Javed, U., Kubistin, D., Martinez, M., Pollmann, J., Rudolf, M., Parchatka, U., et al. (2019). Laser-induced fluorescence-based detection of atmospheric nitrogen dioxide and comparison of different techniques during the PARADE 2011 field campaign. *Atmospheric Measurement Techniques*, *12*(3), 1461–1481. https://doi.org/10.5194/amt-12-1461-2019

Kenagy, H. S., Sparks, T. L., Ebben, C. J., Wooldrige, P. J., Lopez-Hilfiker, F. D., Lee, B. H., et al. (2018). NO_x lifetime and NO_y partitioning during WINTER. *Journal of Geophysical Research: Atmospheres*, *123*, 9813–9827. https://doi.org/10.1029/2018JD028736

Kercher, J. P., Riedel, T. P., & Thornton, J. A. (2009). Chlorine activation by N_2O_5: Simultaneous, in situ detection of $ClNO_2$ and N_2O_5 by chemical ionization mass spectrometry. *Atmospheric Measurement Techniques*, *2*(1), 193–204. https://doi.org/10.5194/amt-2-193-2009

Kiendler-Scharr, A., Mensah, A. A., Friese, E., Topping, D., Nemitz, E., Prevot, A. S. H., et al. (2016). Ubiquity of organic nitrates from nighttime chemistry in the European submicron aerosol. *Geophysical Research Letters*, *43*, 7735–7744. https://doi.org/10.1002/2016GL069239

Knote, C., Brunner, D., Vogel, H., Allan, J., Asmi, A., Äijälä, M., et al. (2011). Towards an online-coupled chemistry-climate model: Evaluation of trace gases and aerosols in COSMO-ART. *Geoscientific Model Development*, *4*(4), 1077–1102. https://doi.org/10.5194/gmd-4-1077-2011

Lee, B. H., Lopez-Hilfiker, F. D., Mohr, C., Kurtén, T., Worsnop, D. R., & Thornton, J. A. (2014). An iodide-adduct high-resolution time-of-flight chemical-ionization mass spectrometer: Application to atmospheric inorganic and organic compounds. *Environmental Science and Technology*, *48*(11), 6309–6317. https://doi.org/10.1021/es500362a

Lee, B. H., Lopez-Hilfiker, F. D., Veres, P. R., McDuffie, E. E., Fibiger, D. L., Sparks, T. L., et al. (2018). Flight deployment of a high-resolution time-of-flight chemical ionization mass spectrometer: Observations of reactive halogen and nitrogen oxide species. *Journal of Geophysical Research: Atmospheres*, *123*, 7670–7686. https://doi.org/10.1029/2017JD028082

Lee, L., Wooldridge, P. J., Gilman, J. B., Warneke, C., de Gouw, C., & R. C. (2014). Low temperatures enhance organic nitrate formation: Evidence from observations in the 2012 Uintah Basin Winter Ozone Study. *Atmospheric Chemistry and Physics*, *14*(22), 12,441–12,454. https://doi.org/10.5194/acp-14-12441-2014

McDuffie, E. E., Fibiger, D. L., Dubé, W. P., Lopez Hilfiker, F., Lee, B. H., Jaeglé, L., et al. (2018). $ClNO_2$ yields from aircraft measurements during the 2015 WINTER campaign and critical evaluation of the current parameterization. *Journal of Geophysical Research: Atmospheres*, *123*, 12,994–13,015. https://doi.org/10.1029/2018JD029358

McDuffie, E. E., Fibiger, D. L., Dubé, W. P., Lopez-Hilfiker, F., Lee, B. H., Thornton, J. A., et al. (2018). Heterogeneous N_2O_5 uptake during winter: Aircraft measurements during the 2015 WINTER campaign and critical evaluation of current parameterizations. *Journal of Geophysical Research: Atmospheres*, *123*, 4345–4372. https://doi.org/10.1002/2018JD028336

Middlebrook, A. M., Bahreini, R., Jimenez, J. L., & Canagaratna, M. R. (2012). Evaluation of composition-dependent collection efficiencies for the Aerodyne aerosol mass spectrometer using field data. *Aerosol Science and Technology*, *46*(3), 258–271. https://doi.org/10.1080/02786826.2011.620041

Neuman, J. A., Huey, L. G., Dissly, R. W., Fehsenfeld, F. C., Flocke, F., Holecek, J. C., et al. (2002). Fast-response airborne in situ measurements of HNO_3 during the Texas 2000 Air Quality Study. *Journal of Geophysical Research*, *107*(D20), 4436. https://doi.org/10.1029/2001JD001437

Orsini, D. A., Ma, Y., Sullivan, A., Sierau, B., Baumann, K., & Weber, R. J. (2003). Refinements to the particle-into-liquid sampler (PILS) for ground and airborne measurements of water soluble aerosol composition. *Atmospheric Environment*, *37*(9-10), 1243–1259. https://doi.org/10.1016/S1352-2310(02)01015-4

Paul, D., Furgeson, A., & Osthoff, H. T. (2009). Measurements of total peroxy and alkyl nitrate abundances in laboratory-generated gas samples by thermal dissociation cavity ring-down spectroscopy. *Review of Scientific Instruments*, *80*(11). https://doi.org/10.1063/1.3258204

Pusede, S. E., Duffey, K. C., Shusterman, A. A., Saleh, A., Laughner, J. L., Wooldridge, P. J., et al. (2016). On the effectiveness of nitrogen oxide reductions as a control over ammonium nitrate aerosol. *Atmospheric Chemistry and Physics*, *16*(4), 2575–2596. https://doi.org/doi:10.5194/acp-16-2575-2016

Ridley, B. A., & Grahek, F. E. (1990). A small, low flow, high sensitivity reaction vessel for NO chemiluminescence detectors. *Journal of Atmospheric and Oceanic Technology*, *7*(2), 307–311.

Rollins, A. W., Pusede, S., Wooldridge, P., Min, K. E., Gentner, D. R., Goldstein, A. H., et al. (2013). Gas/particle partitioning of total alkyl nitrates observed with TD-LIF in Bakersfield. *Journal of Geophysical Research: Atmospheres*, *118*, 6651–6662. https://doi.org/10.1002/jgrd.50522

Rollins, A. W., Smith, J. D., Wilson, K. R., & Cohen, R. C. (2010). Real time in situ detection of organic nitrates in atmospheric aerosols. *Environmental Science & Technology*, *44*(14), 5540–5545. https://doi.org/10.1021/es100926x

Romer, P. S., Duffey, K. C., Wooldridge, P. J., Allen, H. M., Ayres, B. R., Brown, S. S., et al. (2016). The lifetime of nitrogen oxides in an isoprene-dominated forest. *Atmospheric Chemistry and Physics*, *16*(12), 7623–7637. https://doi.org/10.5194/acp-16-7623-2016

Sander, S. P., Abbatt, J., Barker, J. R., Burkholder, J. B., Friedl, R. R., Golden, D. M., et al. (2011). Chemical kinetics and photochemical data for use in atmospheric studies, Evaluation No. 17, *JPL Publication 10-6*, Jet Propulsion Laboratory, Pasadena. http://jpldataeval.jpl.nasa.gov

Schroder, J. C., Campuzano-Jost, P., Day, D. A., Shah, V., Larson, K., Sommers, J. M., et al. (2018). Sources and secondary production of organic aerosols in the northeastern US during WINTER. *Journal of Geophysical Research: Atmospheres*, *123*, 7771–7796. https://doi.org/10.1029/2018JD028475

Sobanski, N., Schuladen, J., Schuster, G., Lelieveld, J., & Crowley, J. N. (2016). A five-channel cavity ring-down spectrometer for the detection of NO_2, NO_3, N_2O_5, total peroxy nitrates and total alkyl nitrates. *Atmospheric Measurement Techniques*, *9*(10), 5103–5118. https://doi.org/10.5194/amt-9-5103-2016

Stith, J. L., Ramanathan, V., Cooper, W. A., Roberts, G. C., DeMott, P. J., Carmichael, G., et al. (2009). An overview of aircraft observations from the Pacific Dust Experiment campaign. *Journal of Geophysical Research*, *114*, D05207. https://doi.org/10.1029/2008JD010924

Thaler, R. D., Mielke, L. H., & Osthoff, H. D. (2011). Quantification of nitryl chloride at part per trillion mixing ratios by thermal dissociation cavity ring-down spectroscopy. *Analytical Chemistry*, *83*(7), 2761–2766. https://doi.org/10.1021/ac200055z

Thieser, J., Schuster, G., Schuladen, J., Phillips, G. J., Reiffs, A., Parchatka, U., et al. (2016). A two-channel thermal dissociation cavity ring-down spectrometer for the detection of ambient NO_2, RO_2NO_2 and $RONO_2$. *Atmospheric Measurement Techniques*, *9*(2), 553–576. https://doi.org/10.5194/amt-9-553-2016

Thornton, J. A., Wooldridge, P. J., & Cohen, R. C. (2000). Atmospheric NO_2: In situ laser-induced fluorescence detection at parts per trillion mixing ratios. *Analytical Chemistry*, *72*, 528–539. https://doi.org/10.1021/ac9908905

Thornton, J. A., Wooldridge, P. J., Cohen, R. C., Williams, E. J., Hereid, D., Fehsenfeld, F. C., et al. (2003). Comparisons of in situ and long path measurements of NO_2 in urban plumes. *Journal of Geophysical Research*, *108*(D16), 4496. https://doi.org/10.1029/2003JD003559

Wagner, N. L., Dubé, W. P., Washenfelder, R. A., Young, C. J., Pollack, I. B., Ryerson, T. B., & Brown, S. S. (2011). Diode laser-based cavity ring-down instrument for NO_3, N_2O_5, NO, NO_2 and O_3 from aircraft. *Atmospheric Measurement Techniques*, *4*(6), 1227–1240. https://doi.org/10.5194/amt-4-1227-2011

Walega, J., Dye, J., Grahek, F., & Ridley, B. (1991). A compact measurement system for the simultaneous determination of NO, NO_2, NO_y and O_3 using a small aircraft. *Proc. SPIE 1433. Measurement of Atmospheric Gases*, *1433*, 232–241. https://doi.org/10.1117/12.46167

Washenfelder, R. A., Dubé, W. P., Wagner, N. L., & Brown, S. S. (2011). Measurement of atmospheric ozone by cavity ring-down spectroscopy. *Environmental Science & Technology*, *45*(7), 2938–2944. https://doi.org/10.1021/es103340u

Wendel, G. J., Stedman, D. H., Cantrell, C. A., & Damrauer, L. (1983). Luminol-based nitrogen dioxide detector. *Analytical Chemistry*, *55*(6), 937–940. https://doi.org/10.1021/ac00257a027

Wild, R. J., Edwards, P. M., Dubé, W. P., Baumann, K., Edgerton, E. S., Quinn, P. K., et al. (2014). A measurement of total reactive nitrogen, NO_y, together with NO_2, NO, and O_3 via cavity ring-down spectroscopy. *Environmental Science and Technology*, *48*(16), 9609–9615. https://doi.org/10.1021/es501896w

Womack, C. C., Neuman, J. A., Veres, P. R., Eilerman, S. J., Brock, C. A., Decker, Z. C. J., et al. (2017). Evaluation of the accuracy of thermal dissociation CRDS and LIF techniques for atmospheric measurement of reactive nitrogen species. *Atmospheric Measurement Techniques*, *10*(5), 1911–1926. https://doi.org/10.5194/amt-10-1911-2017

Wood, E. C., Wooldridge, P. J., Freese, J. H., Albrecht, T., & Cohen, R. C. (2003). Prototype for in situ detection of atmospheric NO_3 and N_2O_5 via laser-induced fluorescence. *Environmental Science & Technology*, *37*(24), 5732–5738. https://doi.org/10.1021/es034507w

Wooldridge, P. J., Perring, A. E., Bertram, T. H., Flocke, F. M., Roberts, J. M., Singh, H. B., et al. (2010). Total Peroxy Nitrates (ΣPNs) in the atmosphere: The Thermal Dissociation-Laser Induced Fluorescence (TD-LIF) technique and comparisons to speciated PAN measurements. *Atmospheric Measurement Techniques*, *3*(3), 593–607. https://doi.org/10.5194/amt-3-593-2010